

Algorithmic Collusion under Observed Demand Shocks

Zexin Ye *

May 29, 2025

Abstract

The growing reliance on AI-driven pricing algorithms has raised antitrust concerns, particularly that third-party use of nonpublic competitor data may facilitate information sharing and undermine market competition. This paper examines a setting in which firms receive demand information from a common third party and incorporate it into their pricing algorithms. Specifically, I analyze the pricing behavior of Q-learning agents when demand shocks are observable. The simulation results show that at high discount factors, agents consistently charge constant supracompetitive prices across demand states, resulting in price rigidity. This pricing pattern is sustained through collusive strategies that effectively punish deviations and feature a discontinuous switch from punishment back to cooperation. At medium discount factors, however, agents lower prices during booms to reduce incentives to deviate and raise them during downturns, resulting in countercyclical pricing consistent with Rotemberg and Saloner (1986). The findings highlight both the pricing adaptability of Q-learning to fluctuating market demand and the robustness of algorithmic collusion. Compared to settings with unobserved demand shocks, demand observability reduces firm profits and enhances consumer surplus, suggesting that access to market information under algorithmic pricing does not necessarily harm consumers.

Keywords: algorithmic collusion, observed demand shocks, price rigidity, countercyclical pricing, information disclosure

JEL Codes: C63, D21, D43, D83, L13

*ye.754@osu.edu, Department of Economics, The Ohio State University. I would like to thank Huanxing Yang for his valuable advice. I am also grateful to Yonghong An, Yaron Azrieli, Paul J. Healy, and Lixin Ye for their insightful comments. I thank Bill Wang for helpful discussions, and I also appreciate the worthwhile feedback from the OSU Theory/Experimental Reading Group. All errors remain my own.

1 Introduction

In recent years, as pricing algorithms have become widely used across industries, concerns have grown among researchers and policymakers about their impact on competition and consumer welfare (Calvano et al., 2020; see Assad et al., 2021 for a comprehensive review).¹ One antitrust concern is that third-party intermediaries aggregate nonpublic data from competing firms to infer underlying market conditions and generate price recommendations, a form of information sharing that may facilitate price coordination and undermine competition. A prominent example comes from the U.S. rental housing market, where many landlords have adopted commercial pricing software developed by RealPage. RealPage collects proprietary data such as apartment prices and occupancy rates from subscribing landlords and uses this information to estimate market demand and recommend rental rates. This widespread adoption has contributed to inflated rental prices, affecting millions of households and adding an estimated \$3.8 billion to annual rental expenditures. In response, a lawsuit has been filed against RealPage, and legislative efforts have been undertaken to prevent algorithmic facilitation in the rental housing market.² Furthermore, a broader legislative initiative is underway, aiming to prevent algorithmic collusion by prohibiting the use of nonpublic competitor data in pricing algorithms: “It shall be unlawful for a person to use or distribute any pricing algorithm that uses, incorporates, or was trained with nonpublic competitor data.”³

On the research side, a growing body of studies has shown that AI-powered pricing algorithms can autonomously learn to sustain tacit collusion and charge supracompetitive prices without any information sharing (Calvano et al., 2020; Klein, 2021; Calvano et al., 2021). However, the impact of shared demand information on algorithmic pricing remains an open question. On the one hand, more predictable demand reduces uncertainty stemming from

¹Notable providers of algorithmic pricing software include, for example, A2i Systems, Kalibrate, Digonex, NielsenIQ, and RELEX Solutions.

²For the lawsuit, see <https://www.justice.gov/archives/opa/media/1364976/dl?inline>. For the Senate bill, see <https://www.congress.gov/bill/118th-congress/senate-bill/3692>.

³See <https://www.congress.gov/bill/118th-congress/senate-bill/3686>.

demand shocks, allowing algorithms trained on historical data to learn more precise mappings from demand states to optimal prices and to better infer competitors' strategies from observed outcomes, which may, in turn, facilitate collusive coordination. On the other hand, more informative demand signals may strengthen the incentive to deviate during booms, as the immediate gain from undercutting collusive prices may outweigh the expected future losses from punishment, thereby undermining the sustainability of collusion.

Motivated by these policy concerns and the existing research gap, this paper examines how access to demand information affects market outcomes in a setting where firms delegate pricing decisions to algorithms. Firms cannot directly observe stochastic demand shocks and instead rely on a third party that processes their nonpublic data and provides signals about current demand. Specifically, the third party is assumed to perfectly predict the current demand state and fully disclose this information to subscribing firms. The firms then integrate this demand information into their pricing algorithms.⁴ Thus, this setup allows me to adopt the framework of Rotemberg and Saloner (1986) to examine algorithmic pricing when demand shocks are observable. In the model, two agents engage in an infinitely repeated Bertrand competition game with a homogeneous good, where an i.i.d. demand shock occurs in each period. At the beginning of each period, agents observe the realized demand state and then simultaneously set prices. They also observe their rivals' past prices, making this a setting with perfect monitoring.

Both agents are played by identical Q-learning algorithms, which are commonly used in previous studies on algorithmic pricing. Q-learning is a fundamental algorithm in reinforcement learning, valued for its simplicity and model-free design.⁵ I modify the Q-learning algorithm to incorporate the current realized demand state, enabling the algorithms to observe and respond to demand shocks, with technical details presented in the section of Ex-

⁴Such third parties are typically more professional and efficient at estimating market demand than individual firms, not only because they have access to nonpublic data from subscribers, but also due to their use of more advanced estimation methods, specialized personnel, and economies of scale (Harrington Jr, 2025).

⁵Reinforcement learning (RL) has become a foundational technique in modern artificial intelligence, with industry leaders such as OpenAI and ByteDance actively deploying RL-based frameworks to develop advanced AI systems. See Sutton (2018) for a comprehensive introduction to RL.

perimental Design.

My main findings are threefold. First, when agents are sufficiently patient (i.e., the discount factor is high), Q-learning agents consistently charge constant prices across demand states, resulting in price rigidity. This stands in contrast to procyclical pricing predicted by Rotemberg and Saloner (1986).⁶ Under rigid pricing, agents autonomously learn collusive strategies and achieve supracompetitive profits without explicit programming or communication. The deviation tests reveal that, for any possible price undercut from any demand state, the expected losses outweigh the expected gains, and the probability of profitable deviations consistently remains low. This suggests that Q-learning agents successfully resist stronger incentives to deviate during booms. Hence, algorithmic collusion persists under observed demand shocks. Moreover, price dynamics along the deviation path show that, following an initial deviation, prices remain low until reaching “restart points” that trigger a swift return to the pre-deviation level. This reflects a discontinuous switch between punishment and cooperation phases, in stark contrast to the gradual return observed in Calvano et al. (2020).

Second, when the discount factor is at a medium level, countercyclical pricing becomes predominant instead of rigid pricing, consistent with the prediction of Rotemberg and Saloner (1986). Specifically, Q-learning agents correctly recognize that high prices are not sustainable during positive demand shocks and respond by proactively lowering prices, while maintaining relatively high prices during downturns. Furthermore, the robustness analysis reveals that a necessary condition for sustaining countercyclical pricing is that both agents observe the demand shocks. In an asymmetric setting where only one agent incorporates demand information, countercyclical pricing breaks down. The informed agent’s low prices during booms are misinterpreted by the uninformed agent as deviations, triggering price wars across demand states and ultimately resulting in uniformly low prices.

Third, the comparative statics reveal that pricing algorithms generate lower profits un-

⁶The divergence stems from whether past realized demand states are included in the state variables. For further discussion, see the section of Symmetric Rigid Pricing.

der observed demand shocks compared to unobserved ones, although algorithmic collusion arises in both settings. While the effect of improved demand forecasting on consumer welfare is theoretically ambiguous (Sugaya and Wolitzky, 2018; Miklós-Thal and Tucker, 2019; O’Connor and Wilson, 2021), this paper finds that demand observability increases consumer surplus under algorithmic pricing. This finding suggests that restrictions on data sharing may not effectively deter collusion and could even undermine market competition. Accordingly, the results support the critique by Harrington Jr (2025) that such regulatory approaches are unlikely to constitute an effective remedy.

To the best of my knowledge, this is the first paper to examine how pricing algorithms operate in a setting where demand information is shared across firms. The results highlight both the robustness of algorithmic collusion and the adaptability of Q-learning to market fluctuations. The latter finding echoes recent empirical evidence from the U.S. multifamily rental market, where Calder-Wang and Kim (2023) show that commercial pricing algorithms make rents more responsive to changing demand conditions.⁷ Furthermore, this paper provides simulation-based support for the pooling (rigid pricing) scheme, rather than the sorting scheme, as a collusion device.⁸ Thus, in the context of AI-powered pricing, price rigidity is not merely a theoretical curiosity, but a plausible emergent pattern of algorithmic coordination. The broader policy implications are discussed in the conclusion.

The rest of the paper is organized as follows. Section 2 provides a review of the literature. Section 3 introduces the economics environment for simulation and then explains in detail the modified Q-learning algorithms that can observe demand shocks. Section 4 describes how to derive long-run price cycles, based on which I analyze pricing patterns, evaluate performance and conduct deviation tests. Section 5 conducts a number of robustness checks.

⁷In contrast to the countercyclical pricing identified in this paper, Calder-Wang and Kim (2023) document a procyclical response: firms using algorithmic pricing reduce rents rapidly during downturns and raise them during recoveries. This difference is likely driven by the higher competitiveness in the multifamily rental market compared to the oligopolistic setting studied here.

⁸Classic theoretical models show that collusion can be sustained when firms pool states by maintaining constant prices (Athey et al., 2004; Hanazono and Yang, 2007). Empirical and experimental studies provide supporting evidence as well (Campbell and Eden, 2014; Fonseca and Normann, 2012).

Section 6 concludes.

2 Literature Review

This research relates to three strands of literature. First, it contributes to the growing body of work on collusion sustained by pricing algorithms. The pioneering study by Calvano et al. (2020) investigate how Q-learning algorithms behave in a general Bertrand competition model with both vertical and horizontal differentiation. Their results show that Q-learning agents autonomously learn to set supracompetitive prices, maintained through collusive strategies that effectively deter deviations. In a dynamic sequential pricing framework adapted from Maskin and Tirole (1988), where firms set prices in turn, Klein (2021) demonstrates that Q-learning agents can still achieve stable collusion. Calvano et al. (2021) build on the framework of Green and Porter (1984), in which firms face unobserved stochastic demand shocks and cannot perfectly monitor rivals' behavior.⁹ They show that Q-learning agents are still able to sustain tacit collusion, confirming that imperfect monitoring is not an obstacle to algorithmic collusion.¹⁰ This paper contributes by showing that when demand shocks are observable, Q-learning algorithms can resist the temptation to deviate during booms and consistently sustain collusion.

Second, this paper contributes to an important strand of the collusion literature that examines how demand information influences collusive outcomes. Rotemberg and Saloner (1986) study a setting in which the demand shock is modeled as i.i.d. and publicly observed. They show that when firms are sufficiently patient, they can sustain the first-best collusive outcome by charging the monopoly price in each demand state, resulting in procyclical pricing—prices rise during booms and fall during downturns. However, when the

⁹In this setting, firms cannot distinguish whether low prices are driven by negative demand shocks or by rivals' production expansion.

¹⁰For other recent studies on this topic, to name a few, Assad et al. (2024) provide empirical evidence that the widespread introduction of algorithmic pricing in Germany's retail gasoline market significantly raises profit margins and thereby softens competition. Fish et al. (2024) show that agents powered by Large Language Models can sustain autonomous collusion without explicit instructions. Ballester (2021) demonstrates that algorithmic collusion can also arise in a setting of sequential pricing with stochastic costs.

discount factor is lower, the incentive to deviate during booms becomes sufficiently strong that firms must reduce prices to mitigate the temptation to undercut. As a result, unlike Green and Porter (1984), Rotemberg and Saloner (1986) predict that price wars occur during booms rather than downturns. In some cases, prices in booms may even fall below those in downturns, leading to countercyclical pricing, where prices move in the opposite direction of the economic cycle. Subsequent research extends this literature by relaxing the i.i.d. assumption on demand shocks (Kandori, 1991; Haltiwanger and Harrington Jr, 1991; Bagwell and Staiger, 1997; Knittel and Lepore, 2010). In contrast, with the development of AI-powered techniques for demand forecasting, recent studies by Miklós-Thal and Tucker (2019) and O'Connor and Wilson (2021) examine how improved demand prediction, in the form of more precise signals about the current demand state, affects collusive behavior. This paper contributes by comparing collusive outcomes across different information structures, specifically between settings where demand shocks are either observable or unobservable, when firms delegate pricing to algorithms. It further shows that Q-learning algorithms can adapt their pricing strategies to changing market conditions, with some patterns aligning with theoretical predictions and others driven by specific features of pricing algorithms.

In a broader context, this study relates to the growing literature at the intersection of economics and artificial intelligence. For example, in the context of platform design, Johnson et al. (2023) show that when sellers use pricing algorithms, platforms can design demand-steering rules (such as dynamic price-directed prominence) to effectively destabilize algorithmic collusion, thereby improving consumer welfare and increasing platform revenue. Dolgoplov (2024) and Xu and Zhao (2024) demonstrate that reinforcement learning agents can learn to cooperate or collude under certain conditions, depending on their learning rules and the structure of the game. This paper integrates reinforcement learning into an industrial organization framework, offering new insights into how AI agents behave in repeated pricing games and their implications for competition policy in algorithmically mediated markets.

3 Experimental Design

3.1 Economic Environment

Two agents engage in an infinitely repeated Bertrand competition game, each producing a homogeneous product under linear demand.¹¹ In every period t , a random common demand shock θ_t occurs, shifting the market demand curve parallelly. This shock is i.i.d. and follows a uniform distribution over $[\underline{\theta}, \bar{\theta}]$; Both agents first observe the realized θ_t , and then set their prices simultaneously. Let $\mathbf{p}_t = (p_{1t}, p_{2t})$ be the complete price profile and p_{-it} be the rival price. The demand for agent i at period t is given by

$$D_{it}(p_{it}, p_{-it}, \theta_t) = \begin{cases} b + \theta_t - p_{it} & \text{if } p_{it} < p_{-it} \\ \frac{b + \theta_t - p_{it}}{2} & \text{if } p_{it} = p_{-it} \\ 0 & \text{if } p_{it} > p_{-it} \end{cases}$$

where b is the coefficient of market demand. Correspondingly, the period payoff for agent i at period t is $\pi_{it} = (p_{it} - c_i)D_{it}(p_{it}, p_{-it}, \theta_t)$, where c_i is the constant marginal cost.

Dynamic Problem In this modified repeated game, agent i 's problem is to maximize the expected present value of the payoff stream $\mathbb{E}[\sum_{t=0}^{\infty} \delta^t \pi_{it}]$ with discount factor δ . Agent i 's problem can be modelled as a Markov decision process, in which the agent chooses price p_{it} based on state s_t . The value function for agent i is

$$V_i(s) = \max_{p_i \in A} \left\{ \pi_i + \delta \mathbb{E}[V_i(s') | s, p_i] \right\} \quad (1)$$

where s' is the next state and A is the action (price) space.

¹¹Eliminating product differentiation facilitates a more tractable analysis of countercyclical pricing.

Action Q-learning requires a finite action space. Therefore, I discretize the action space into m equally spaced points within $[\underline{p}^C, \bar{p}^M]$, where \underline{p}^C is the Bertrand equilibrium price under $\underline{\theta}$ and \bar{p}^M is the monopoly price under $\bar{\theta}$.

State The state s_t should contain two key components. First, it should include the current realized demand state θ_t , allowing agents to observe and respond to market fluctuations. Second, under perfect monitoring, it should include past prices to enable agents to detect and punish deviations so that tacit collusion can be sustained.

To prevent the state space from growing indefinitely, the model employs a bounded memory of K periods. This means agents only remember the prices from the last K periods.¹² The resulting state s_t is given by

$$s_t = \{\mathbf{p}_{t-1}, \dots, \mathbf{p}_{t-K}, \theta_t\}.$$

Notably, past realized demand states are excluded from s_t .¹³ This specification is grounded in three theoretical justifications: (i) given that demand shocks are i.i.d., past realizations provide no predictive value for the current state θ_t ; (ii) past shocks neither influence the current period payoff nor help detect deviations; and (iii) excluding past shocks reduces the state space dimensionality, which improves computational efficiency and facilitates learning.

¹²This restriction is supported by both simulation evidence (Calvano et al., 2020) and theoretical results. Barlo et al. (2009) and Barlo et al. (2016) prove folk theorems with bounded memory in infinite and finite action spaces, respectively.

¹³Including past realizations of demand shocks in s_t does not affect the sustainability of collusion but alters the predominant pricing pattern (see the Discussion in Section 4.2).

3.2 Q-Learning Algorithms

The value function can be expressed in terms of a Q-function that represents the expected discounted value (Q-value) associated with selecting price p in state s , as follows

$$Q_i(s, p) = \pi_i + \delta \mathbb{E} \left[\max_{p' \in A} Q_i(s', p') \mid s, p \right] \quad (2)$$

where the first term on the right-hand side is the period payoff and the second term is the expected continuation value.¹⁴ Since S and A are finite, the Q-function can be represented as an $|S| \times |A|$ matrix, where each entry in the Q-matrix \mathbf{Q}_i stores the corresponding Q-value $Q_i(s, p)$.

However, the Q-matrix \mathbf{Q}_i cannot be solved directly, since the period payoff $\pi_i(p_i, p_{-i}, \theta)$ depends on the rival's pricing decision, and the transition function $F_i(s' \mid s, p)$ remains unknown to agent i . Thus, I employ the Q-learning algorithm, first proposed by Watkins (1989), to address this challenge.

Learning Equation The Q-learning algorithm estimates the Q-matrix through an iterative procedure. At the beginning of period t , agent i observes θ_t and thus s_t is determined. Then each agent simultaneously chooses its price p_{it} , after which the period payoff π_{it} is realized.¹⁵ At the end of period t , agent i updates the corresponding cell (s_t, p_{it}) in \mathbf{Q}_{it} , through the learning equation:

$$Q_{it+1}(s, p) = (1 - \alpha)Q_{it}(s, p) + \alpha \left[\pi_{it} + \delta \int_{\theta} \max_{p' \in A} Q_{it}(s', p') h(\theta) d\theta \right] \quad (3)$$

where the new $Q_{it+1}(s, a)$ combines the previous value with the current reward π_{it} plus the expected discounted continuation value. The weight $\alpha \in [0, 1]$ is called the learning rate. Although each agent remembers the last K -period prices, the next state s' is uncertain due

¹⁴The relationship between the Q-function and the value function is $V(s) \equiv \max_{p \in A} Q(s, p)$.

¹⁵The action selection rule will be introduced next.

to randomness of upcoming demand shocks.¹⁶ A key assumption here is that agents know the distribution of demand shocks, i.e., the density function $h(\theta)$. Given this, they compute the expected discounted future value by integrating over all possible realizations of θ_{t+1} .

An alternative updating rule is the sample-based approach, in which $Q_{it+1}(s, p)$ is updated in period $t + 1$, after observing the realized demand shock θ_{t+1} but before choosing the next price p_{t+1} .¹⁷ In contrast, this paper adopts the expectation-based updating rule introduced above. The primary motivation is that it better reflects the timing structure of the repeated game: learning takes place at the end of period t , before θ_{t+1} is realized, and therefore should rely only on currently available information. In addition, the expectation-based rule requires only knowledge of the distribution over future demand states and does not rely on a structural transition function, thereby preserving the model-free nature of Q-learning.¹⁸ This aligns with the assumption in Rotemberg and Saloner (1986) that the distribution of demand shocks is commonly known. In practice, this assumption is plausible: firms or third-party intermediaries typically have access to extensive historical data and are able to reliably estimate demand distributions prior to deploying pricing algorithms.

For all other cells $s \neq s_t$ and $p \neq p_{it}$, the Q-value remains unchanged: $Q_{t+1}(s, p) = Q_t(s, p)$. Thus, Q-learning updates only one cell of the Q-matrix at a time.

Action Selection The classic ε -greedy rule, which has been effective in approximating the true Q-matrix (Calvano et al., 2020; Klein, 2021), is adopted to determine the price charged

¹⁶The state s_{t+1} is $\{\mathbf{p}_{t-K+1}, \dots, \mathbf{p}_t, \theta_{t+1}\}$, where the last K -period prices are remembered but θ_{t+1} has not yet been realized at period t .

¹⁷The robustness checks report simulation results based on sample-based update.

¹⁸Although the expectation-based update relies on the known distribution of demand shocks, the transition probability $F_i(s' | s, p)$ remains unknown due to strategic uncertainty: each agent's next state and payoff depend on the other agent's independent action. As a result, the learning process remains fundamentally model-free.

by each agent in every period:

$$p_{it} \begin{cases} = \operatorname{argmax}_{p \in A} Q_{it}(s_t, p) & \text{with the prob. } 1 - \varepsilon_t \\ \sim \text{Uniform}(A) & \text{with the prob. } \varepsilon_t \end{cases} \quad (4)$$

where $\varepsilon_t = e^{-\beta t}$ is a time-declining exploration rate that effectively balances between exploration and exploitation. In each period, the agent selects either the price that yields the highest Q-value (exploitation mode with probability $1 - \varepsilon_t$) or samples a price uniformly at random (exploration mode with probability ε_t).¹⁹

Initialization The initialization of Q-matrix \mathbf{Q}_0 possesses degrees of freedom. In the baseline setting, \mathbf{Q}_0 is initialized to reflect the fact that at $t = 0$ of each session, each agent operates in full exploration mode ($\varepsilon_0 = 1$) and thus samples uniformly from the discrete price space.²⁰ An alternative initialization is also examined in robustness checks.

3.3 Parameters

In the baseline setting, the market size is $b = 6$ and the marginal cost for each agent is $c_i = 0$. The i.i.d. demand shock θ takes values in $\{0, 4\}$ with equal probability. These two demand states are denoted as low (L) and high (H), respectively, representing the negative and positive demand shocks. Under these conditions, the one-shot Bertrand competition equilibrium price is $p_L^C = p_H^C = 0$, while the monopoly prices are $p_L^M = 3$ and $p_H^M = 5$ for the low and high demand states. The theoretical prediction of pricing patterns across δ in the infinitely repeated setting is provided in Appendix D.

The action space A is discretized into 11 equally-spaced points over the interval $[0, 5]$, such that $A = \{0, 0.5, \dots, 5\}$.²¹ For computational simplicity, the algorithm employs a one-

¹⁹Early on, the ε -greedy rule favors exploration to learn about the environment. As learning progresses, it gradually shifts toward exploitation, selecting prices with the highest current Q-values.

²⁰For details of the calculation, see Appendix C.

²¹Under discretization, there exists an additional one-shot symmetric equilibrium—both agents charge the

period memory ($K = 1$). The cardinality of the state space is thus $|S| = 242$. The state at period t is $s_t = (p_{1t-1}, p_{2t-1}, \theta_t)$.

To ensure consistent learning and sufficient exploration, following Calvano et al. (2020), I adopt a learning rate of $\alpha = 0.15$ and an exploration rate of $\beta = 4 \times 10^{-6}$ for the baseline model. A wide range of α and β is also examined in robustness checks. The discount factor δ is varied from 0.60 to 0.99 with an increment of 0.01, enabling a comprehensive analysis of the impact of time preferences on pricing behavior. For each parameter configuration (α, β, δ) , I conduct 1,000 simulation sessions, each serving as an independent observation.

A sketch of one simulation session is presented in Algorithm 1 below.

Algorithm 1 Pricing Simulation Procedure for One Session

First step: Initialization

1: \mathbf{Q}_{i0} is generated

Second step: Loop

2: **while** convergence criterion is not satisfied **do**

3: θ_t is realized

4: $s_t = (p_{1t-1}, p_{2t-1}, \theta_t)$

5: p_{it} is determined through the action selection rule (4)

6: $\pi_i(p_{it}, p_{-it}, \theta_t)$ is realized

7: $\mathbf{Q}_i(s, p)$ is updated through the learning equation (3)

Single Demand State For comparison, I also conduct simulations without demand uncertainty by fixing the demand state at L and H, respectively.

Convergence While Q-learning convergence in single-agent problems has been proven under certain conditions (Watkins and Dayan, 1992), convergence in strategically interdependent environments remains theoretically unguaranteed. Following Calvano et al. (2020), I employ an empirical convergence criterion: learning is considered complete when each player’s optimal strategy remains unchanged for 100,000 consecutive periods.²² The same price of 0.5 across both demand states.

²²Specifically, convergence is achieved when the optimal price $p_{it}(s) = \operatorname{argmax}_{p \in A} Q_i(s, p)$ for each player i and state s remains constant over 100,000 consecutive iterations.

lution terminates upon meeting this criterion or reaching one billion iterations, whichever occurs first. Under the baseline parameters $\alpha = 0.15$ and $\beta = 4 \times 10^{-6}$, the average number of iterations required for convergence is 2,331,775.²³

4 Results

Similar to previous research, this paper analyzes agents' pricing behavior after learning is completed, rather than investigating how algorithms converge to their limit strategies. In this section, I first explain the methodology for deriving pricing patterns from the limit strategies. Then, I evaluate the performance of these pricing patterns in terms of prices and profits and assess whether they are capable of sustaining tacit collusion.

4.1 Pricing Patterns

4.1.1 Limit Strategy

The limit strategy for agent i is the optimal policy derived from the converged Q-matrix, which maps each state to its optimal price, formally defined as

$$p_i^*(s) = \operatorname{argmax}_{p \in A} Q_i(s, p), \quad \forall s \in S \quad (5)$$

Directed Graph Using the limit strategies $p_1^*(s)$ and $p_2^*(s)$, I construct a directed network to represent the state-price dynamics. Consider a directed graph $G = (V, g)$, where $V = \{1, 2, \dots, M\}$ is the set of nodes.²⁴ Each node $v = (\theta, p_1, p_2)$ represents a combination of the current demand state and prices charged by each agent. The adjacency matrix g is an $M \times M$ matrix with each element $g_{ij} \in \{0, 1\}$ denoting whether a directed edge exists between nodes

²³Convergence at the single demand states L and H requires 1,700,681 and 1,901,235 iterations, respectively. The smaller number of iterations is expected, as the state space under each single demand state decreases by half.

²⁴Note that $M = 242$.

i and j .²⁵ A directed edge exists (i.e., $g_{ij} = 1$) in G if and only if the prices in node v_j are optimal responses prescribed by the limit strategies, given the previous prices in node v_i and the current demand state in node v_j . Note that it's possible to have $g_{ii} = 1$, which means that if the demand state remains the same from one period to the next, agents do not change their optimal prices, resulting in a self-loop.

4.1.2 The Long-run Price Cycle

Price dynamics are expected to converge to a long-run price cycle G_c , a subgraph of G . In other words, once price dynamics enter G_c , all subsequent price movements remain forever in G_c .

The long-run price cycle G_c must satisfy two requirements. First, G_c must be a strongly connected component (SCC), meaning that any node in G_c can reach any other node through directed paths.²⁶ Second, each node in G_c must have all its direct successors within G_c . This ensures that random demand shocks cannot cause exits from G_c .²⁷ By construction, G_c is absorbing, as no path exists from any node in G_c to nodes outside it.²⁸

Figure 1 illustrates various examples of G_c with different node counts. The label within each node indicates the demand state and the price pair. Directed edges represent transitions between nodes, while an arrow that loops back to the same node represents a self-loop. For example, Figure 1a shows a simple case where G_c contains two nodes. Each node has two outgoing edges: one to the other node and one self-loop. This structure reveals that both agents charge the price of 3 regardless of demand shocks.

²⁵In a directed network, g_{ij} generally does not equal g_{ji} .

²⁶To identify SCCs in G , I employ the algorithm from Tarjan (1972), as modified by Nuutila and Soisalon-Soininen (1994).

²⁷The number of outgoing edges for each node equals the number of possible demand states, which is two in the baseline model.

²⁸One potential issue is that multiple cycles might exist in G . Since 99.94% of sessions contain exactly one cycle, this has virtually no impact on results.

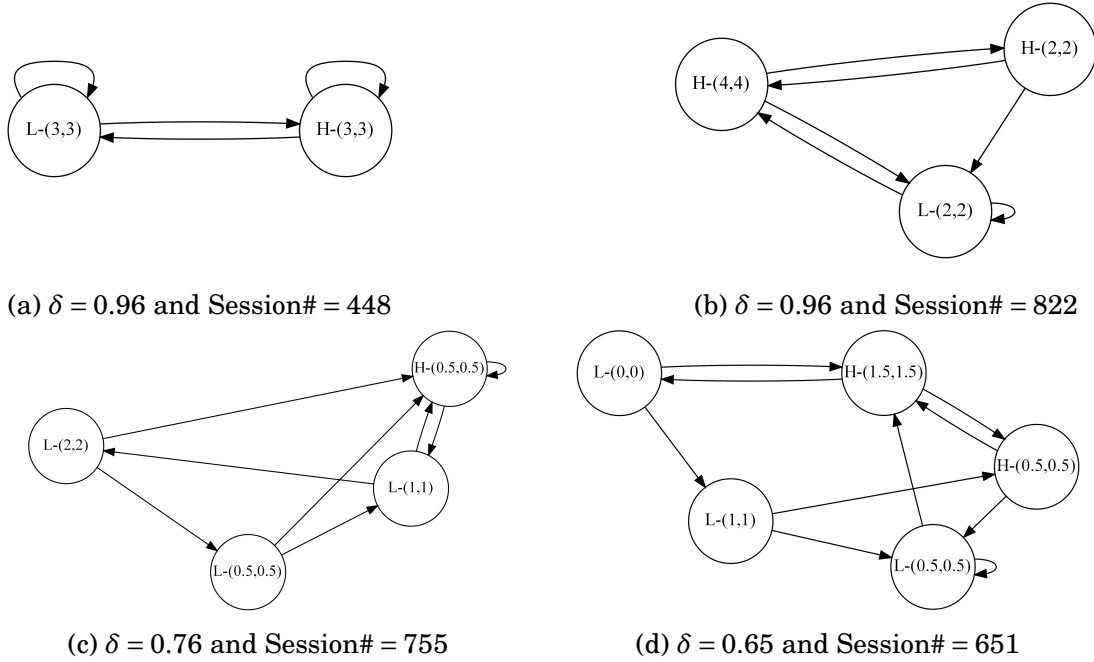


Figure 1: Examples of G_c with Varying Numbers of Nodes

4.1.3 Steady-state Price

The price dynamics on G_c follow a finite-state Markov process. Using its stationary distribution, I compute the average long-run price at each demand state. Details of the derivation are provided in Appendix E. Based on these average long-run prices, I define the pricing patterns as follows.

Definition 1 A long-run price cycle G_c exhibits symmetric and rigid pricing (Sym-Rigid) if it consists of exactly two nodes and maintains identical prices across both agents and demand states.

Definition 2 A long-run price cycle G_c exhibits procyclical pricing (Pro-Cycle) if the average long-run prices charged by both agents are strictly higher at H than at L.

Definition 3 A long-run price cycle G_c exhibits countercyclical pricing (Counter-Cycle) if the average long-run prices charged by both agents are strictly higher at L than at H.

The two-node constraint is imposed in Sym-Rigid because allowing more than two nodes would necessarily lead to price variation across demand states, thereby violating price rigidity. In contrast, the characterization of Pro-Cycle and Counter-Cycle is based on average long-run prices and does not depend on the number of nodes. This allows for local price variations while capturing the fundamental relationship between prices and demand conditions.

Table 1 below summarizes the definitions of each pricing pattern.

Table 1: Definitions of Pricing Patterns

Name	Abbreviation	Pricing
Symmetric and Rigid Pricing	Sym-Rigid	$p_1^L = p_2^L = p_1^H = p_2^H$ (exactly 2 nodes)
Procyclical Pricing	Pro-Cycle	$p_1^H > p_1^L$ and $p_2^H > p_2^L$
Countercyclical Pricing	Counter-Cycle	$p_1^L > p_1^H$ and $p_2^L > p_2^H$

Notes: p_i^θ denotes agent i 's average long-run price at demand state θ .

4.1.4 Distribution of Pricing Patterns

Figure 2 shows the distribution of the pricing patterns Sym-Rigid, Pro-Cycle, and Counter-Cycle across different values of δ .²⁹ When δ is low, Sym-Rigid dominates, with prices close to 0.5. As δ increases to medium levels (approximately 0.70 to 0.85), Counter-Cycle becomes the most prevalent pricing pattern. When δ is high, Sym-Rigid again emerges as the most frequent pattern, with prices increasing alongside δ . Specifically, when $\delta \geq 0.95$, Sym-Rigid accounts for over 40% of sessions.

In the following analysis, I focus primarily on the predominant pricing patterns, namely Sym-Rigid at high δ and Counter-Cycle at medium δ , and also compare them with other identified pricing patterns.

²⁹For detailed price dynamics across δ , see Figure A.2 in Appendix.

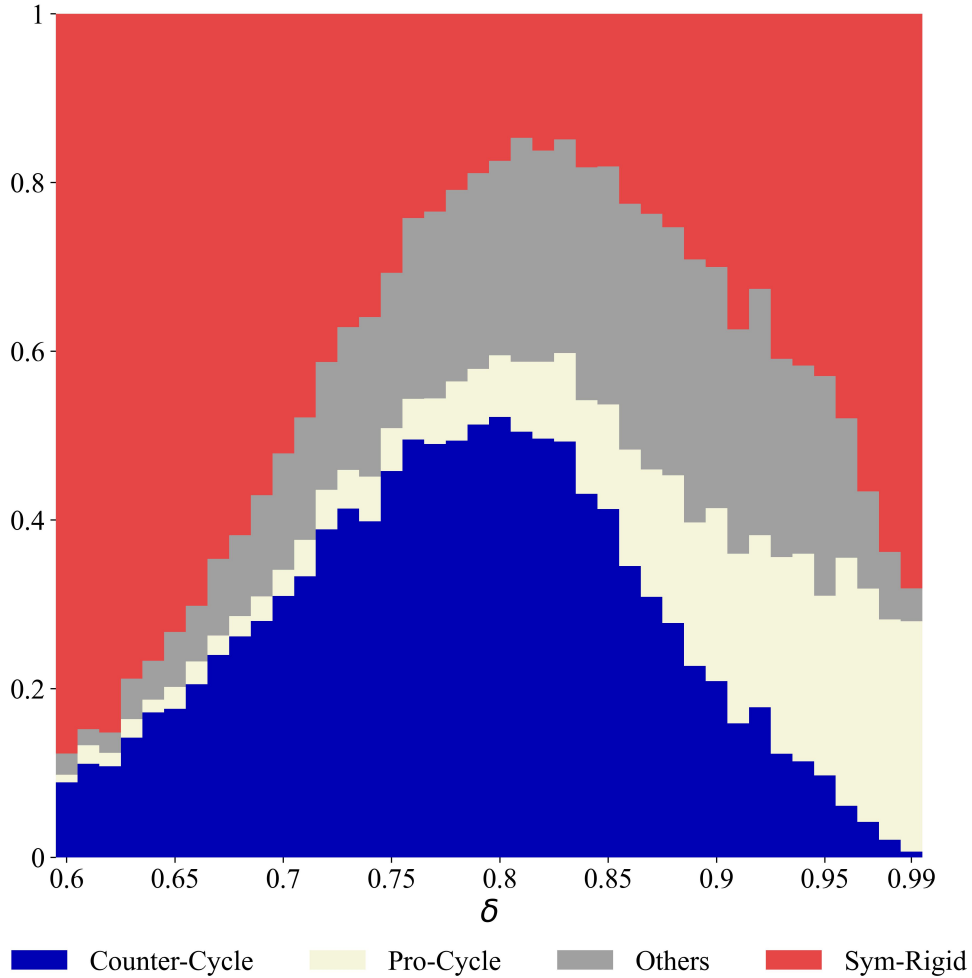


Figure 2: Distribution of Pricing Patterns across δ

4.2 Symmetric Rigid Pricing

4.2.1 Performance

Table 2 summarizes prices and profits under several pricing patterns at $\delta = 0.96$. In Panel A, prices under Sym-Rigid remain constant at 2.64 across both demand states and agents, representing 88% and 53% of the monopoly prices at L and H, respectively. The expected profit across demand states exceeds 80% of the equally split monopoly profit (i.e., the first-best collusive outcome). Under Pro-Cycle, the average price at H is higher than that under Sym-Rigid, yet it does not yield higher profits. This is because Pro-Cycle exhibits asymmetric pricing in most sessions, where agents charging higher prices lose the entire market and

earn zero profit. The presence of pricing asymmetry, combined with a lower average price at L, reduces the overall expected profit to 69% of the split monopoly profit—significantly lower than that under Sym-Rigid (t-test, p-value = 0). The superior performance of Sym-Rigid helps explain why Q-learning converges to it more frequently than to Pro-Cycle (0.48 vs. 0.29).

Table 2: Summary Statistics of Pricing Patterns when $\delta = 0.96$

Category	Ratio ^a	p^L	p^H	π^L	π^H	Expected Profit ^b
<i>Panel A: Under Demand Shocks</i>						
Sym-Rigid	0.48	2.64 (0.88 ^c)	2.64 (0.53)	4.25 (0.94)	9.53 (0.76)	6.89 (0.81)
Pro-Cycle ^d	0.29	2.13 (0.71) [1.49 ^e]	2.98 (0.60) [2.69]	2.85 (0.63)	8.86 (0.71)	5.85 (0.69)
<i>Panel B: At Single Demand State</i>						
Sym-1Node ^f	0.93, 0.97 ^g	2.14 (0.71)	3.09 (0.62)	4.04 (0.90)	10.48 (0.84)	7.26 (0.85)

Notes: a. Frequency of the corresponding pricing pattern among all sessions.

b. Average profit across both demand states.

c. Proportion relative to the monopoly price or the equally split monopoly profit.

d. Pro-Cycle may involve asymmetric pricing. However, as average prices and profits are nearly identical for both agents, Panel A shows only agent 1's results.

e. Average effective market price.

f. Sym-1Node denotes the symmetric pricing pattern at the single demand state, where G_c contains exactly one node and both agents charge the same price.

g. These two numbers refer to the frequencies of Sym-1Node at single demand states L and H, respectively.

To further evaluate Sym-Rigid, I examine Q-learning agents' pricing behavior in the absence of demand shocks. Panel B reports prices and profits for the symmetric pricing pattern, denoted as Sym-1Node, under each single demand state.³⁰ Under Sym-1Node, agents charge 2.13 at L and 3.09 at H. In comparison, Sym-Rigid's constant price of 2.66 lies between them, smoothing prices across demand states. This price smoothing yields an expected profit comparable to the average profit across both single demand states (0.81 vs. 0.85, relative to the split monopoly profit).

³⁰The symmetric pricing pattern refers to the long-run price cycle G_c containing exactly one node where both agents charge the same price.

Figure A.3 in Appendix compares Sym-Rigid and Sym-1Node across values of δ . As δ increases, the expected profit under Sym-Rigid gradually approaches the average profit under Sym-1Node. Notably, at $\delta = 0.99$, the average price under Sym-Rigid rises to 3.31, exceeding the monopoly price at L. Its expected profit reaches 7.55, which corresponds to 96.2% of the average profit under Sym-1Node.

Result 1: When δ is high, Sym-Rigid emerges as the predominant pricing pattern, occurring more frequently than Pro-Cycle and yielding supracompetitive profits. Compared to settings with single demand states, Sym-Rigid smooths prices across demand states, and its expected profit converges to that of Sym-1Node as δ increases.

4.2.2 Analysis of Collusion

Although Sym-Rigid can maintain supracompetitive profits under high δ , this alone is not sufficient to conclude collusion. As defined by Harrington (2018), collusion occurs when firms use strategies that incorporate a reward–punishment scheme, which rewards a firm for abiding by the supracompetitive outcome and punishes any deviation from it. While each agent’s strategy can be derived from the Q-matrix, as noted by Calvano et al. (2020), fully describing these strategies is challenging due to the numerous contingencies and the variation in strategies across different sessions. Therefore, to address this challenge, I follow the method proposed by Calvano et al. (2020) to conduct the deviation test.

However, the presence of (observed) demand shocks complicates the deviation test. In the absence of demand shocks, each price undercut results in a unique and deterministic deviation path. In contrast, with demand shocks, the uncertainty over future demand states gives rise to multiple possible deviation paths following a price undercut. To illustrate this difference, Figure 3 displays two single-path deviations in the absence of demand shocks, where the demand state remains at H. In contrast, Figure 4 presents a multi-path deviation triggered by an undercut at H in the presence of demand shocks.

In Figure 4, the stable price in G_c is 4, depicted by the two rightmost nodes with self-

loops and mutual arrows. The leftmost node represents the initial deviation, where agent 1 undercuts by 0.5 upon observing that the current demand state is H. The intermediate nodes and connecting arrows illustrate the multiple possible paths leading from this deviation back to G_c .³¹

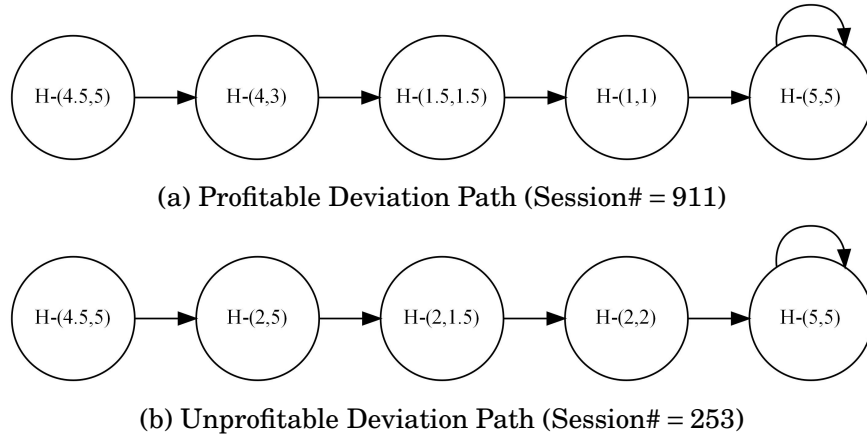


Figure 3: Two Single-path Deviations at Single Demand State H

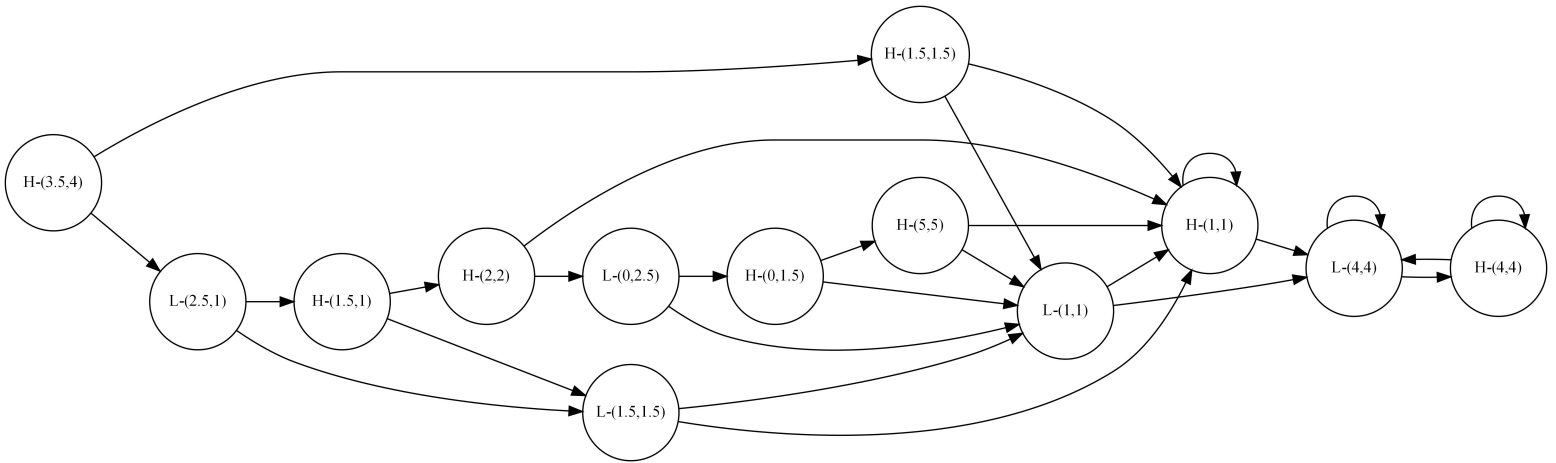


Figure 4: A Multi-path Deviation under Demand Shocks (Deviation Occurs at H and Session# = 513)

To address this randomness, I conduct one thousand simulations for each deviation scenario, defined as a specific combination of the price undercut level, the identity of the deviating agent, and the initial demand state at which the deviation occurs. In each simulation,

³¹For instance, one deviation path is $H-(3.5,4) \rightarrow H-(1.5,1.5) \rightarrow H-(1,1) \rightarrow L-(4,4)$, with a length of 4.

one agent is forced to deviate unilaterally from G_c by undercutting the stable price in the initial period, while the other agent still charges the stable price. After this initial deviation, both agents follow their limit strategies until the price dynamics return to G_c . Throughout this deviation path—from the initial undercut until the return to G_c —I record both the realized profits on the deviation path and the counterfactual profits that would have been earned had both agents remained in G_c (i.e., the non-deviation path). For each path, the accumulated discounted profit is averaged over one thousand simulations, and the resulting average is treated as a single observation. I then compare the average discounted profits along the deviation and non-deviation paths to assess whether the deviation scenario is profitable. Algorithm 2 in Appendix provides a detailed description of the deviation simulation procedure.

Table 3 summarizes results from deviation tests when agent 1 undercuts by the smallest price unit (i.e., 0.5), which generates the highest initial deviating profit in most cases.³² Panel A shows that under Sym-Rigid, the deviating agent’s profit ratios (deviation path relative to non-deviation path, denoted as $\% \Pi_1$) are 0.81 and 0.91 when deviation occurs at L and H, respectively. This indicates that the losses from deviation outweigh the gains. The frequencies of profitable deviations (denoted as q^D) are 0.17 at L and 0.31 at H, implying that deviations are unprofitable approximately 80% and 70% of cases. The higher frequency when deviation happens at H stems from the larger initial gain from undercutting.³³ Thus, both the low frequencies of profitable deviations and the profit ratios below one indicate that such price undercutting is unprofitable.³⁴

I further extend the deviation analysis to all undercutting levels. Table A.1 in Appendix reports the frequencies of profitable deviations for the deviating agent at each price undercut. These frequencies are consistently low and decrease rapidly toward zero as the mag-

³²The results of deviation tests remain nearly identical regardless of which agent initiates the deviation. Therefore, for illustration purposes, I present the results from forcing agent 1 to undercut.

³³From another perspective, conditional on the deviating agent’s profit ratio being below one, more than 80% of Sym-Rigid sessions fall within this category.

³⁴The procyclical pricing pattern, however, does not pass the deviation tests. Possible explanations are discussed in Section 4.3.

nitude of undercut increases. Additionally, Table A.2 in Appendix presents the profit ratios for each feasible price undercut, with all ratios below one. Taken together, these results demonstrate that deviations are unprofitable across all possible levels of undercutting.

Table 3: Summary Statistics for Deviation Tests when $\delta = 0.96$

Agent 1 undercuts by 0.5		Deviation occurring at L			Deviation occurring at H			
Category	length ^a	q ^D (freq.) ^b	% Π_1 (deviator) ^c	% Π_2 (non-deviator) ^d	length	q ^D (freq.)	% Π_1 (deviator)	% Π_2 (non-deviator)
<i>Panel A: Under Demand Shocks</i>								
Sym-Rigid	7.54	0.17	0.81	0.55	7.56	0.31	0.91	0.47
<i>Panel B: At Single Demand State</i>								
Sym-1Node	4.53	0.24	0.89	0.49	4.91	0.21	0.87	0.47

Notes: Panel A displays results from deviation tests under demand shocks; Panel B presents those results at each single demand state, L and H.

a. Average periods for price dynamics returning to G_c .

b. Frequency of profitable deviations.

c. The deviating agent's profit ratio: deviation path relative to non-deviation path.

d. The non-deviating agent's profit ratio: deviation path relative to non-deviation path.

Last, an interesting pattern emerges when comparing scenarios with and without demand shocks. Panel B in Table 3 presents the results of deviation tests conducted at each single demand state.³⁵ When deviations occur at L, profitable deviations are less frequent under demand shocks (0.17 vs. 0.24; t-test, p-value = 0). Conversely, at H, they are more frequent (0.31 vs. 0.21; t-test, p-value = 0). The intuition is as follows: deviations at L trigger price wars in both demand states, increasing expected losses. In contrast, deviations at H spread future losses across demand states, mitigating the overall loss.

Result 2: The deviation tests show that under Sym-Rigid, for any price undercut from any demand state, the expected gains from deviation are outweighed by the expected losses, making profitable deviations unlikely for either agent. As a result, algorithmic collusion emerges under observed demand shocks. This lack of profitability reflects a punishment

³⁵Deviation tests also show that deviations are unprofitable at each single demand state. For results across all possible undercuts, see Panel B in Table A.1 and Table A.2 in Appendix. The frequencies of profitable deviations without demand shocks are higher than those reported in Calvano et al. (2020), primarily because this paper assumes homogeneous products, whereas Calvano et al. (2020) incorporate product differentiation. With homogeneous products, price competition is more intense, as an undercutting agent captures the entire market, thereby generating greater gains from deviation.

mechanism implemented by the non-deviating agent, which effectively suppresses the deviator’s payoff along the deviation path.

4.2.3 Features of Deviation Path

Following the deviation test, I explore the price dynamics along the deviation path and summarize three representative features.

Probabilistic profitability of deviations. Under demand shocks, multi-path deviations make the profitability of a deviation probabilistic, determined by the occurrence rates of profitable paths, rather than deterministic (0 or 1) at single demand states. For example, in Figure 4, two profitable deviation paths have a combined occurrence rate of 18.75%.³⁶ In contrast, Figure 3 illustrates the deterministic case, where one deviation path is profitable and the other is not.

Frequent low-price transitions. The second feature of the deviation path is the frequent occurrence of specific low price pairs before returning to G_c . To quantify their prevalence, I employ the in-degree centrality metric, which measures how often these price pairs are visited.³⁷ Figure 5 displays the average in-degree centrality for each price pair following agent 1’s undercut by the minimum price unit after observing a positive demand shock. The deepest color blocks in the heat maps are concentrated in price ranges from 0.5 to 1.5, indicating these price pairs serve as common transition nodes. These transition nodes play an crucial role in punishment, substantially contributing to the unprofitability of deviations. Notably, one of the two symmetric one-shot equilibria—(0, 0) at both demand states—is rarely used as punishment, possibly because agents recognize that charging the price of 0, while harming

³⁶These two profitable deviation paths are $H-(3.5, 4) \rightarrow H-(1.5, 1.5) \rightarrow L-(1, 1) \rightarrow L-(4, 4)$ and $H-(3.5, 4) \rightarrow L-(2.5, 1) \rightarrow L-(1.5, 1.5) \rightarrow L-(1, 1) \rightarrow L-(4, 4)$, with occurrence rates of 12.5% and 6.25%, respectively.

³⁷The in-degree centrality for a node v in a directed graph is calculated as:

$$C_{D_{in}}(v) = \frac{D_{in}(v)}{V - 1}$$

where $D_{in}(v)$ is the number of edges entering node v and V is the total number of nodes in the graph. The initial deviating nodes are excluded when calculating the in-degree centrality.

their rival, generates no profit for themselves.³⁸ The pattern of frequent low-price transitions remains consistent across different undercut levels, deviating agents, pre-deviation prices, and initial deviating demand states. Figure A.4 in Appendix presents the average in-degree centrality for deviation occurring at L, which is almost identical to Figure 5.

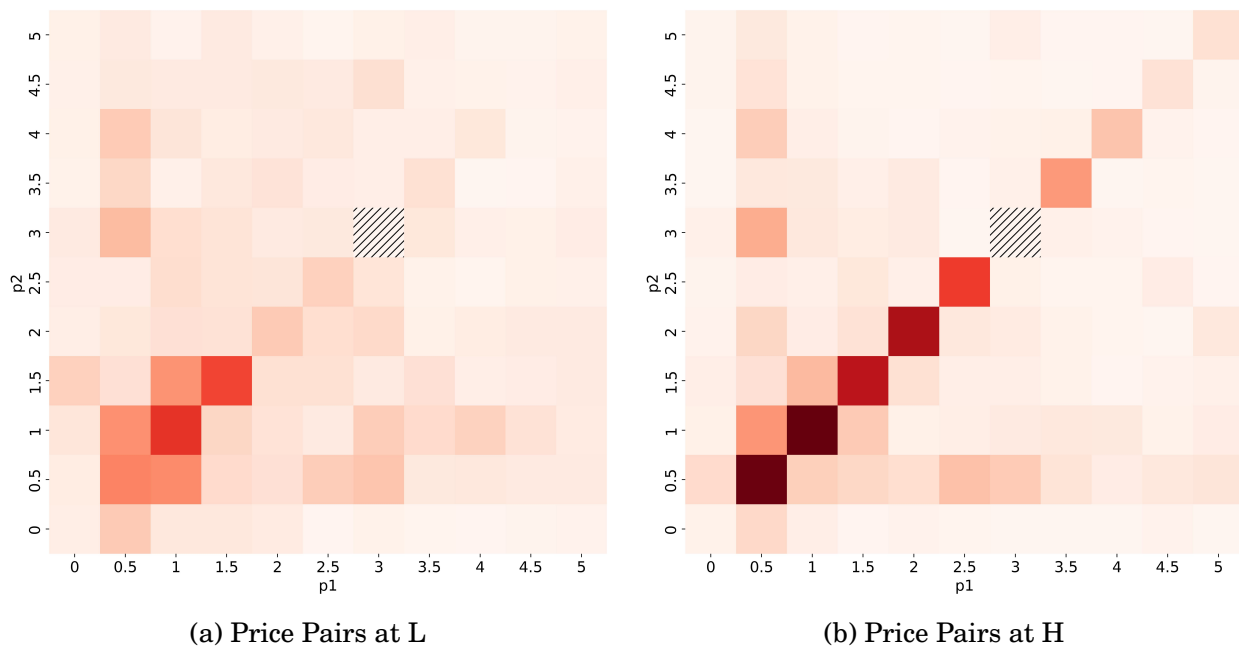


Figure 5: In-Degree Centrality of Price Pairs Along the Deviation Path (Deviation Initiated at H)

Notes: The square depicted in lines marks the pre-deviation price of 3. A deviation occurs when agent 1 undercuts by the minimum price unit after observing a positive demand shock. The color gradient indicates the level of in-degree centrality.

Discontinuous switch. The price dynamics along the deviation path exhibit a discontinuous switch between punishment and cooperation. Upon detecting a deviation, both agents enter a punishment phase, charging low prices regardless of demand states. This phase persists for several periods before prices abruptly return to the pre-deviation level. Figure 6 illustrates a representative example of how prices return to G_c following a unilateral deviation. In the cooperation phase (G_c), both agents charge 3 across both demand states. At $t = 1$, given a positive demand shock, the deviating agent undercuts by 0.5. At $t = 2$, the

³⁸Moreover, those low price pairs at H generally show deeper colors than at L, suggesting higher transition intensity at H.

non-deviating agent responds with punishment by dropping its price to a low level. The deviating agent, anticipating this punishment, also charges low prices. Both agents maintain low prices regardless of demand states during the punishment phase, after which prices abruptly return to G_c . Figure 7 plots the average prices in last four periods of deviation paths initiated by all possible undercuts, further emphasizing the sharp discontinuity between punishment and cooperation phases.

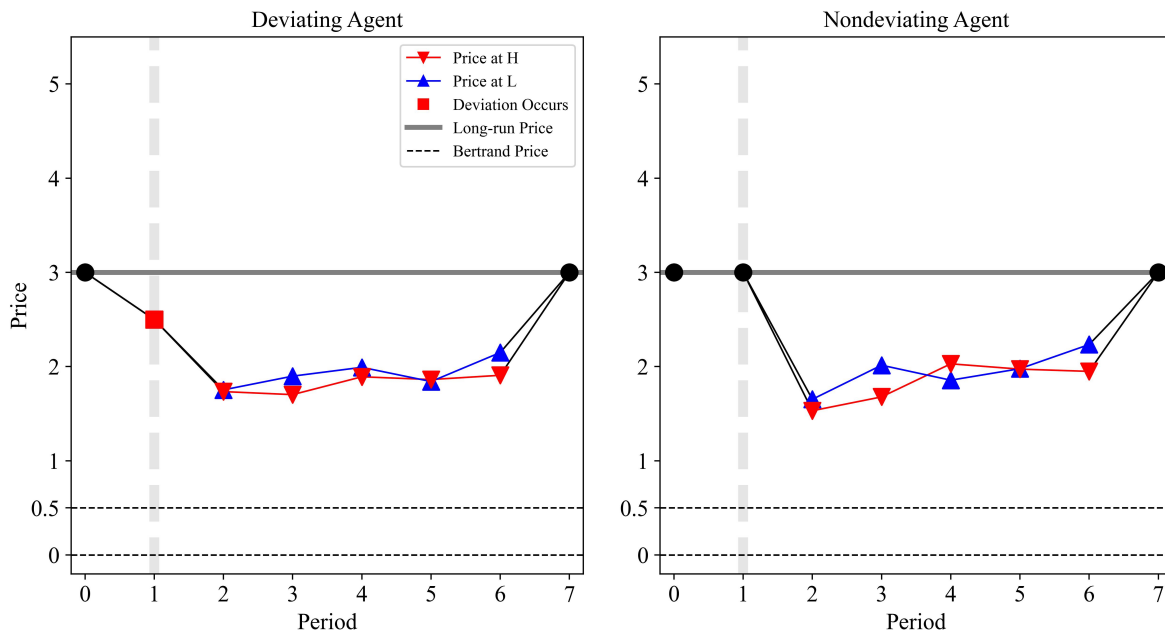


Figure 6: Price Dynamics after Deviation

Notes: The length of the deviation path is fixed at 7 periods, with prices at $t = 0$ and $t = 7$ equal to the pre-deviation price in G_c . For each period and demand state, prices are first averaged across deviation simulations within the same session, and then averaged across all Sym-Rigid sessions. The deviation is initiated at $t = 1$, conditional on the demand state being H.

This discontinuous switch represents a key distinction from Calvano et al. (2020).³⁹ In their setting without demand shocks, prices along the deviation path initially drop and then gradually return to the pre-deviation level. One plausible explanation for the abrupt transition is that Q-learning agents, given observed demand shocks, tend to develop clear “restart points” that, once reached, trigger a swift return to cooperation. This explanation

³⁹A feature shared with Calvano et al. (2020) is that the discontinuous switching pattern still resembles the “stick-and-carrot” strategies of Abreu (1986).

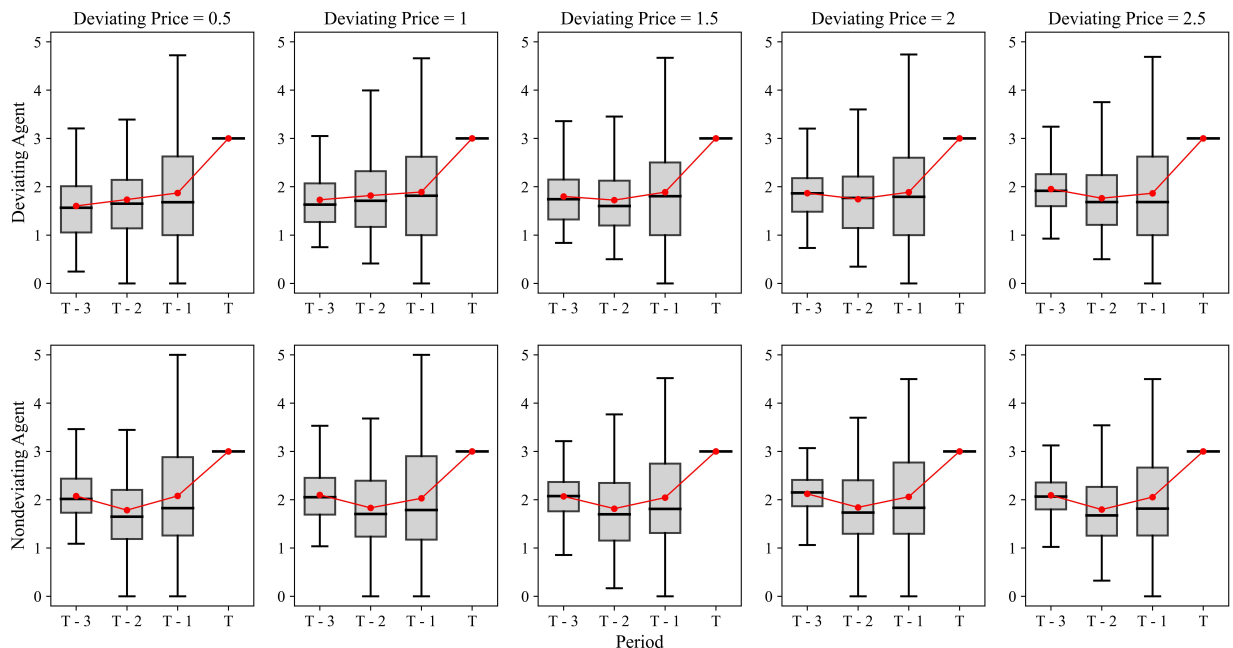


Figure 7: Average Prices in the Last Four Periods Along the Deviation Path

Notes: The figure plots the average prices across demand states and sessions in the last four periods ($T - 3$ to T) along the deviation path. The pre-deviation price is fixed at 3. In each box, the black line indicates the median, and the gray area represents the interquartile range (25th to 75th percentiles). Mean prices are marked with red dots and connected by red lines. The whiskers show the full range of prices.

is economically intuitive. First, when observing a price increase, algorithms may struggle to determine whether it reflects a cooperative intent or merely a response to a positive demand shock. Second, during a gradual recovery, the temptation to deviate may intensify when high prices coincide with favorable demand conditions.

These restart points exhibit two key characteristics: *commonality*, referring to the similarity of restart points across deviation scenarios within a session; and *concentration*, referring to the extent to which a small number of restart points dominate within each deviation scenario. To quantify commonality, I compute the pairwise Jaccard similarity between the sets of restart points associated with different deviation scenarios within each session.⁴⁰ The average pairwise similarity across sessions is 0.85, suggesting that despite variation in when and how agents deviate, they tend to return to cooperation through similar restart

⁴⁰Details of the calculation are provided in Appendix G.

points. To assess concentration, Figure A.5 in the Appendix plots the average proportion of restart points by rank. In particular, the rank-1 proportion exceeds 50%, and the distribution is heavily concentrated within the top three ranks, indicating that a small number of restart points are repeatedly used within each deviation scenario.

Result 3: Multi-path deviations under Sym-Rigid exhibit three representative features: probabilistic profitability of deviations, frequent transitions to low prices, and a discontinuous switch between punishment and cooperation. The third feature is particularly noteworthy: once a deviation is detected, both agents switch to charging low prices across demand states. This punishment phase lasts for several periods, after which the agents abruptly return to cooperation upon reaching specific restart points.

4.2.4 Discussion

An unanswered question is why the predominant pricing pattern is Sym-Rigid rather than Pro-Cycle. This contradicts the theoretical prediction by Rotemberg and Saloner (1986) that agents would charge higher prices during higher demand states at sufficiently high δ . Given that Sym-Rigid accounts for about half of all sessions at $\delta = 0.96$, a more specific question arises: why do algorithms predominantly learn rigid pricing instead of procyclical pricing when restricted to two-node graph structures?

The reason lies in agents' limited memory: recall that they only remember the previous period's price pair, not the accompanying demand state. This algorithmic design cause agents to treat identical price pairs from different demand states as equivalent, making Sym-Rigid more likely to emerge. To illustrate, consider two examples: a symmetric rigid pricing pattern, $L - (3,3)$ and $H - (3,3)$, and a procyclical pricing pattern, $L - (2,2)$ and $H - (4,4)$. Figure 8 represents these two pricing patterns using finite automata. The rigid pricing pattern is characterized by a single state (price pair) with two self-referencing transitions. In contrast, the procyclical pricing pattern requires two distinct states and four transitions, consisting of two inter-state transitions and two intra-state transitions, since it

assigns different price pairs to different demand states. Clearly, rigid pricing involves lower complexity in terms of states and transitions, making it easier for Q-learning to discover and implement.

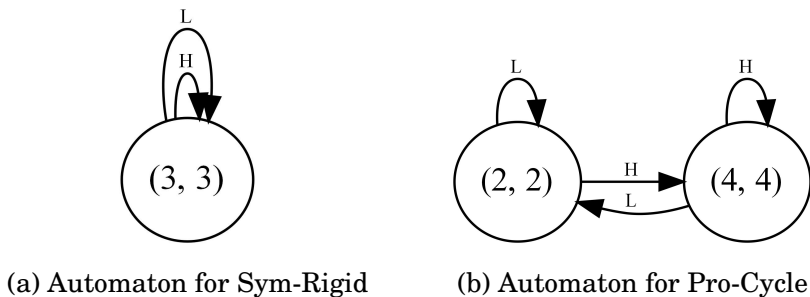


Figure 8: Pricing Patterns Represented by Finite Automata

Following this argument, if agents can remember both the previous period's price pair and the corresponding demand state (extended-state setting), then identical price pairs under different demand states become distinguishable (for example, $L - (3, 3)$ and $H - (3, 3)$ are treated differently). Under this condition, procyclical and rigid pricing exhibit the same level of complexity when constrained to two-node graph structures. Consequently, procyclical pricing should become the predominant pattern for sufficiently high δ , as agents through exploration mode sooner or later discover that charging higher prices at H yields greater profits. The simulation results confirm this prediction.⁴¹ When constrained to two-node graph structures, procyclical pricing appears in 19.2% of all sessions, while rigid pricing accounts for only 2.3%. More broadly, procyclical pricing represents 57.3% of all sessions, demonstrating that the information contained in the state variable s significantly shapes agents' learning outcomes.

However, under the same parameter configuration, agents in the baseline setting (where the previous demand state is not remembered) converge to rigid pricing in 87.9% of sessions and achieve 6.5% higher expected profits compared to those in the extended-state setting.

⁴¹When agents remember the previous period's demand state, the state space doubles compared to the baseline setting. In this case, the parameters are set to $\delta = 0.96$, $\alpha = 0.15$, and $\beta = 1 \times 10^{-6}$. The smaller value of β extends the exploration phase before convergence.

This finding suggests that Sym-Rigid outperforms Pro-Cycle not only in terms of complexity but also in profitability.

4.3 Countercyclical Pricing

4.3.1 Graph Structure

Figure 9 illustrates several examples of long-run price cycles G_c under Counter-Cycle when $\delta = 0.76$. In contrast to Sym-Rigid, which has exactly one node per demand state, G_c under Counter-Cycle typically exhibits multiple nodes at each demand state. As shown in Table 4, when $\delta = 0.76$, the average number of nodes under Counter-Cycle is 5.49 at L and 3.58 at H. Thus, Counter-Cycle is characterized by a larger and more complex graph structure. Although a comprehensive characterization of the graph structure of G_c remains challenging, one thing clearly stands out: the node $H - (0.5, 0.5)$, which is one of the symmetric one-shot equilibria at H, plays a crucial role in contributing to the average lower price observed at H. Three representative features of $H - (0.5, 0.5)$ are summarized below.

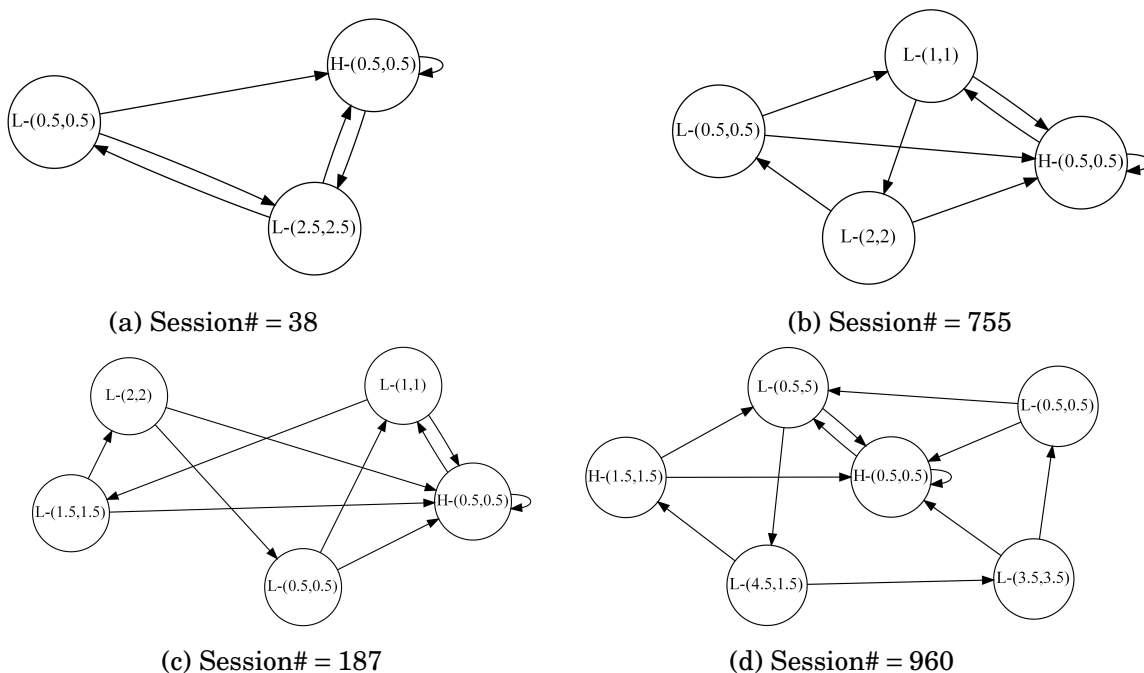


Figure 9: Representative Examples of G_c under Counter-Cycle with $\delta = 0.76$

Table 4: Summary Statistics for G_c under Counter-Cycle with $\delta = 0.76$

Demand State	Obs.	Size ^a	p_1 ^b	p_2	Freq. of (0.5,0.5) ^c
L	495	5.49	2.12	2.09	0.669
H	495	3.58	1.06	1.05	0.998

Notes: a. The average number of nodes of G_c at each demand state.
b. The average price of agent 1 at each demand state.
c. The frequency of the price pair (0.5,0.5) at each demand state.

High frequency. As shown in Table 4, the frequency of $H - (0.5, 0.5)$ is 99.8%, appearing in almost every G_c . In stark contrast, the frequency of $L - (0.5, 0.5)$ diminishes significantly to 66.9%.

High centrality. Figure 10 visualizes the in-degree centrality for price pairs at each demand state when $\delta = 0.76$. $H - (0.5, 0.5)$ stands out with an exceptionally high in-degree centrality, represented by the darkest color block, while all other price pairs show much lighter colors. This visual contrast underscores its uniquely high degree of connectivity within G_c . Simulation tests corroborate such connectivity, showing that starting from any node in G_c , it takes on average less than two periods to reach $H - (0.5, 0.5)$.

High self-loop tendency. Among all price pairs at both demand states, $H - (0.5, 0.5)$ has the highest self-loop frequency at 85.6%, significantly exceeding any other price pair. This characteristic suggests that price dynamics exhibit a strong tendency to persist at $H - (0.5, 0.5)$, conditional on the positive demand shock occurring in the next period.

Result 4: Under Counter-Cycle, $H - (0.5, 0.5)$ appears in nearly every G_c and acts as a strong attractor in the price dynamics, causing other nodes to reach it in fewer than two periods and then remain there (conditional on the positive demand shock in the next period). These features persist throughout the medium range of δ , substantially contributing to the lower average prices at H and creating very limited opportunities for agents to undercut at H.

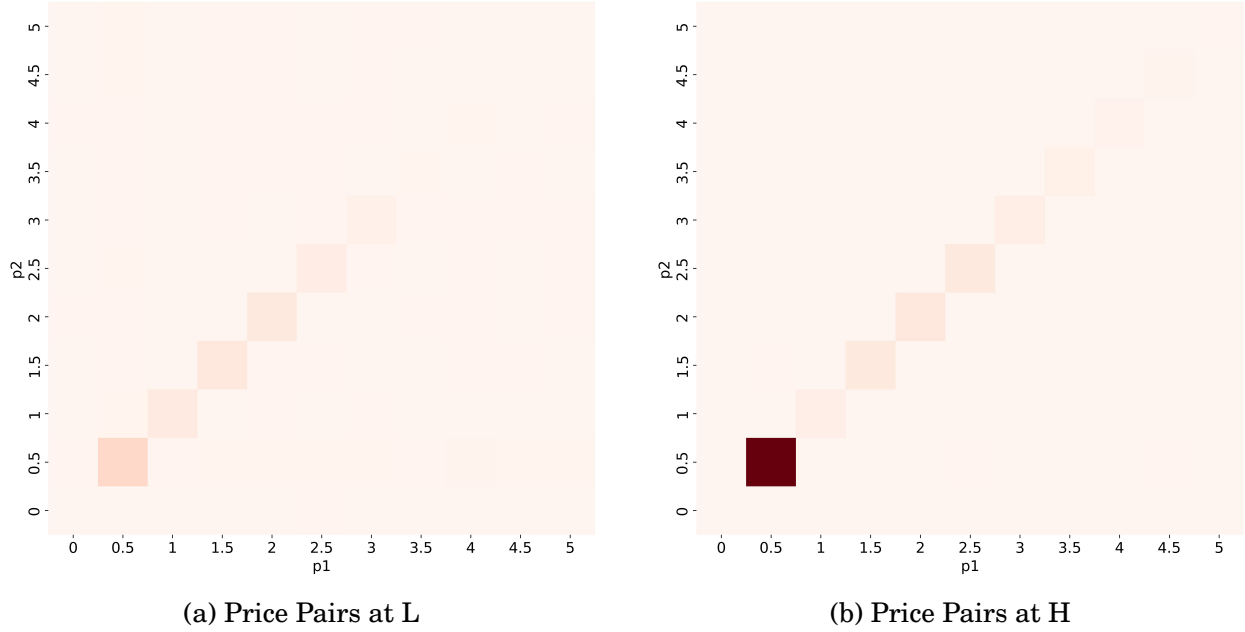


Figure 10: In-Degree Centrality of Price Pairs within G_c under Counter-Cycle

Notes: The color gradient in the figure indicates the level of in-degree centrality, with darker colors representing higher centrality.

4.3.2 Performance

Table 5 presents summary statistics for several pricing patterns at $\delta = 0.76$. Under Counter-Cycle, the average price at L is 2.12, which is 71% of the monopoly price, yielding 61% of the split monopoly profit. This indicates that supracompetitive profit is still maintained during negative demand shocks. In contrast, at H, the average price is only 1.06, representing 21% of the monopoly price and yielding 32% of the split monopoly profit. Overall, the expected profit under Counter-Cycle, attains 40% of the best collusive outcome. While this might appear low, Counter-Cycle still maintains 75% of the average profit achieved across two single demand states (shown in Panel B).

In contrast, under Sym-Rigid, the fixed price of 0.66 is lower than the prices observed under Counter-Cycle for both demand states (and also lower than the effective market prices shown in brackets). Consequently, the expected profit under Sym-Rigid is significantly lower

Table 5: Summary Statistics of Pricing Patterns when $\delta = 0.76$

Category	Ratio	p^L	p^H	π^L	π^H	Expected Profit
<i>Panel A: Under Demand Shocks</i>						
Sym-Rigid	0.24	0.66 (0.22)	0.66 (0.13)	1.70 (0.38)	3.03 (0.24)	2.37 (0.28)
Counter-Cycle	0.50	2.12 (0.71) [1.50]	1.06 (0.21) [0.99]	2.74 (0.61)	4.00 (0.32)	3.37 (0.40)
<i>Panel B: At Single Demand State</i>						
Sym-1Node	0.88, 0.63	0.76 (0.25)	1.79 (0.36)	1.89 (0.42)	7.12 (0.57)	4.51 (0.53)

Notes: The settings are identical to those in Table 2. As prices and profits are nearly identical for agents 1 and 2, results are reported for agent 1 only.

than that achieved under Counter-Cycle.⁴² This performance gap helps explain the emergence of Counter-Cycle as the predominant learning outcome.⁴³

Result 5: In the medium range of δ , Counter-Cycle emerges as the predominant pricing pattern. Under this pricing pattern, Q-learning algorithms successfully coordinate to sustain supracompetitive profits at L but perform poorly at H, generating relatively low expected profits. Nevertheless, Counter-Cycle still significantly outperforms Sym-Rigid, indicating that its emergence as the dominant learning outcome is not a random occurrence.

4.3.3 Analysis of Collusion

Deviation tests are necessary for evaluating collusion under Counter-Cycle, just as they were previously applied to Sym-Rigid. However, within the long-run price cycle G_c under Counter-Cycle, the characteristics of the node $H - (0.5, 0.5)$, particularly its frequent occurrence and traversal, may impede the effective implementation of punishment.

⁴²The p-value of the t-test is 0.

⁴³Figure A.6 in Appendix compares the profits of Counter-Cycle and Sym-Rigid across δ . The comparison reveals a critical threshold at $\delta \approx 0.8$. Below this threshold, Counter-Cycle exhibits superior performance, while Sym-Rigid takes the lead above it. These results indicate that Counter-Cycle generally outperforms Sym-Rigid when δ is not sufficiently high.

From a theoretical perspective, Barlo et al. (2009) argue that Nash reversion on the equilibrium path may disrupt coordination under bounded memory. Specifically, agents cannot distinguish between states on the equilibrium path and those off the path where punishment (i.e., Nash reversion) is taking place. Following this argument, when a deviation occurs, $H - (0.5, 0.5)$ is likely used as punishment.⁴⁴ However, given its features in G_c , playing this node along the deviation path leads price dynamics to return immediately to G_c due to one-period memory. As a result, the deviation path may be too short to support effective punishment, potentially making the deviation profitable. The deviation tests under Counter-Cycle confirm this prediction.

Then a puzzle emerges: if deviations are profitable, why does the countercyclical pricing pattern still predominantly emerge? Two conjectures help explain this phenomenon. First, shortened deviation paths imply that more time is spent in G_c , allowing Q-values to accumulate more frequently for nodes within G_c than for those outside it. Second, the presence of multiple nodes within G_c dilutes the likelihood of deviations occurring at any single node during exploration, thereby increasing its resistance to disruption. Together, these two conjectures reinforce the stability of G_c , making it unlikely for Q-values to shift away from supporting the continuation of G_c .

The second conjecture may help explain why Pro-Cycle, despite failing the deviation tests, can still be sustained. Why such pricing patterns, particularly featuring asymmetric pricing and multiple nodes, are able to generate supracompetitive profits without effective punishment remains an open question and warrants deeper investigation.⁴⁵

Result 6: Counter-Cycle does not pass the deviation tests. This failure is primarily due to the frequent occurrence and traversal of the node $H - (0.5, 0.5)$ within G_c , which prevents agents from effectively using it as a form of punishment along the deviation path.

Nevertheless, Counter-Cycle can still be sustained, which may be attributed to two factors:

⁴⁴The other symmetric one-shot equilibrium, $H - (0, 0)$, is not likely to be chosen as it yields strictly zero profit for both agents, confirmed before in the deviation tests under Sym-Rigid.

⁴⁵For reference, Cho and Williams (2024) analytically show that even after shutting down all explicit collusion channels, collusive outcomes may still be sustained when endogenizing the algorithmic selection process.

more frequent Q-value accumulation within G_c due to shortened deviation paths, and the presence of multiple nodes that disperse deviations during exploration.

4.3.4 Discussion

As shown in Figure 2, Sym-Rigid prevails at both high and low values of δ , while Counter-Cycle dominates at intermediate levels. This pattern suggests that the emergence of Counter-Cycle is not a random outcome, but rather an adaptive response to specific levels of time preference, as captured by δ . Then a natural question rises: how do Q-learning algorithms learn to form countercyclical pricing patterns? In particular, how do they move away from rigid pricing and learn to charge lower prices during periods of high demand?

The underlying mechanism is reminiscent of Rotemberg and Saloner (1986). As δ declines to a medium range, agents place greater weight on immediate rewards. Starting from Sym-Rigid, they gradually discover through exploration that undercutting at H yields higher profits, and thus higher Q-values. As a result, such undercuts become increasingly frequent. In response, the non-deviating agent lowers its price, triggering a price war. This downward pressure leads both agents to adopt progressively lower prices at H.

Meanwhile, during negative demand shocks, undercutting generates far less payoff variability than it does at H. Combined with lower exploration at any individual node (as there are more nodes at L), this prevents the Q-values associated with low prices from surpassing those linked to relatively high prices. Thus, sustaining relatively high prices at L remains feasible, giving rise to countercyclical pricing.

As δ declines further into the low range, agents become increasingly myopic, focusing almost exclusively on immediate rewards and disregarding the expected continuation value. Consequently, even modest gains from deviating at L are quickly reinforced. As the Q-values of deviation increase, the relatively high prices at L become unsustainable, and Sym-Rigid, characterized by uniformly low prices across both demand states and agents, reemerges as the predominant pricing pattern.

5 Robustness Checks

In this section, I examine the robustness of the baseline findings, specifically the identified pricing patterns and tacit collusive outcomes. I also investigate whether the information structure—the observability of demand shocks—affects market outcomes.

5.1 Alternative Initialization

To examine the robustness of the identified pricing patterns to alternative Q-matrix initialization, I set the initial Q-values to zero for both agents. The emerging pricing patterns remain consistent with the baseline findings. Specifically, under the baseline parameters $\alpha = 0.15$ and $\beta = 4 \times 10^{-6}$, Sym-Rigid appears with a frequency of 0.59 at $\delta = 0.96$, while Counter-Cycle emerges with a frequency of 0.45 at $\delta = 0.76$.

5.2 Parameter Variations

I systematically vary the learning rate α and the experimentation parameter β . For both parameters, I construct grids of 10 equally spaced points: $\alpha \in [0.05, 0.5]$ and $\beta \in [10^{-6}, 10^{-5}]$. The range of α captures different balances between incorporating new information and retaining past learning, while the range of β reflects varying levels of exploration during the learning process.

Pricing Patterns Figure 11 presents the distribution of pricing patterns across the parameter space of α and β . In Panel A, Sym-Rigid ($\delta = 0.96$) is the predominant pricing pattern, becoming increasingly common as β decreases. In the region with low values of both α and β , its frequency exceeds 70%. Panel B displays the frequency of Counter-Cycle with $\delta = 0.76$ across parameter combinations. While its overall prevalence is lower than that of Sym-Rigid in Panel A, it nonetheless appears consistently across a substantial portion of

the parameter space.⁴⁶ The results in both panels show that the two predominant pricing patterns, Sym-Rigid at high δ and Counter-Cycle at medium δ , are robust and not artifacts of particular parameter choices.

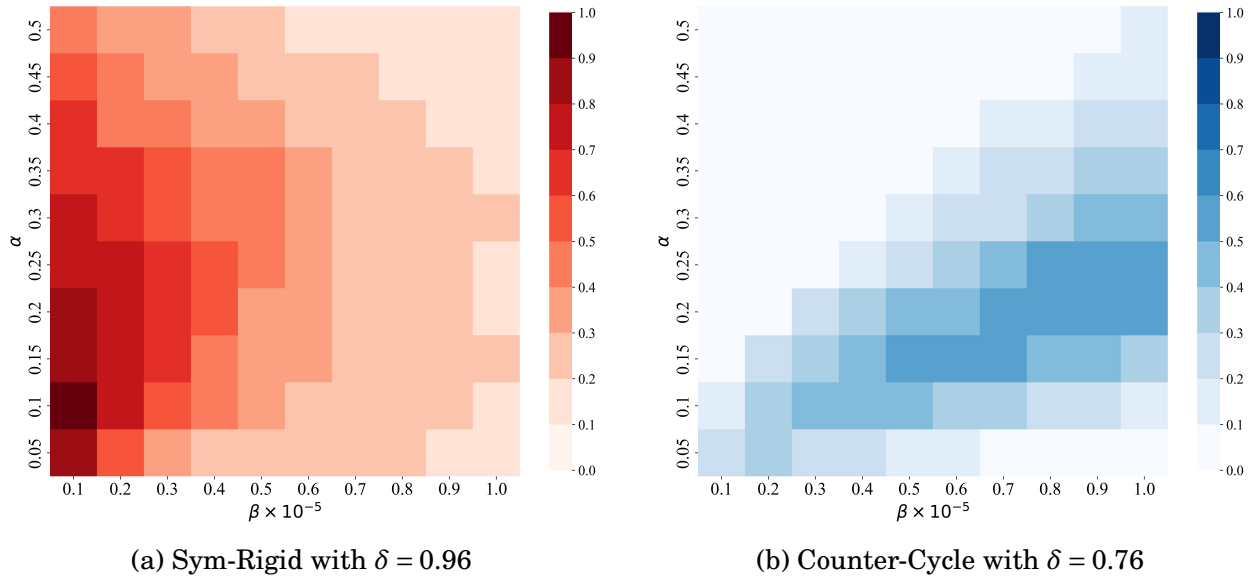


Figure 11: Frequencies of Two Pricing Patterns across Parameter Space

Collusive Profits Figure 12 presents the expected profits under Sym-Rigid ($\delta = 0.96$) as a function of α and β . Across the parameter space, profits range from 65% to 90% of the best collusive outcome and show little sensitivity to changes in the learning and experimentation parameters. The deviation tests also show that deviations are not profitable across this parameter range. These results demonstrate that algorithmic collusion also occurs across an extensive range of parameters, rather than relying on artificial parameter selections.

⁴⁶The prevalence of Counter-Cycle generally remains below 60%, as it competes with Sym-Rigid for dominance at medium levels of δ , with many sessions ultimately converging to the latter. The predominant pattern in the lightest-shaded upper triangle of Panel B is Sym-Rigid.

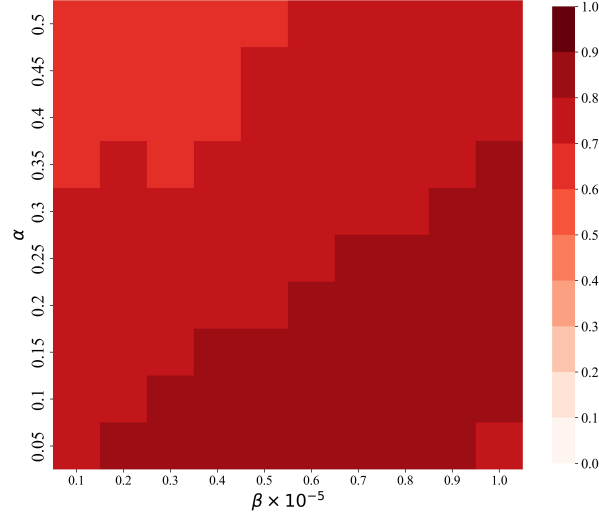


Figure 12: Expected Profits under Sym-Rigid across Parameter Space with $\delta = 0.96$

5.3 Sample-Based Q-learning

I then test the robustness of the baseline findings under sample-based update. The learning equation is given by

$$Q_{it+1}(s, p) = (1 - \alpha)Q_{it}(s, p) + \alpha \left[\pi_{it} + \delta \max_{p' \in A} Q_{it}(s', p') \right] \quad (6)$$

where the update is performed in period $t + 1$, after the realized demand shock θ_{t+1} is observed but before the next-period price p_{t+1} is chosen. Consequently, the future state $s_{t+1} = (p_{1t}, p_{2t}, \theta_{t+1})$ is known at the time of updating.

Table 6 reports the corresponding summary statistics. When $\delta = 0.96$, while Pro-Cycle emerges as the predominant pricing pattern, Sym-Rigid still accounts for a substantial share (28%) and also pass the deviation tests. When $\delta = 0.76$, Counter-Cycle remains predominant, with a share of 66%. Overall, the results suggest that Q-learning agents can sustain algorithmic collusion and adapt their pricing strategies to changing market conditions, regardless of the timing of updates.

Table 6: Summary Statistics with Sample-Based Update

Category	Ratio	p^L	p^H	π^L	π^H	Expected Profit
<i>Panel A: When $\delta = 0.96$</i>						
Sym-Rigid	0.28	2.74 (0.91)	2.74 (0.55)	4.25 (0.94)	9.72 (0.78)	6.99 (0.82)
Pro-Cycle	0.43	2.15 (0.72) [1.54]	2.96 (0.59) [2.70]	2.91 (0.65)	8.88 (0.71)	5.90 (0.69)
<i>Panel B: When $\delta = 0.76$</i>						
Sym-Rigid	0.16	0.55 (0.18)	0.55 (0.11)	1.48 (0.33)	2.59 (0.21)	2.04 (0.24)
Counter-Cycle	0.66	1.65 (0.55) [1.47]	0.73 (0.15) [0.72]	2.83 (0.63)	3.07 (0.25)	2.95 (0.35)

Notes: The settings are identical to those in Table 2. As prices and profits are nearly identical for agents 1 and 2, results are reported for agent 1 only.

5.4 Observability of Demand Shocks

5.4.1 Symmetric Information

The simulation results show that when demand shocks are unobservable, algorithmic collusion and supracompetitive profits remain feasible, echoing Calvano et al. (2020).⁴⁷ In this setting, Sym-1Node—where both agents charge the same price—emerges as the predominant pricing pattern at both $\delta = 0.96$ (73.7%) and $\delta = 0.76$ (58.3%).

Table 7 lists the expected profits of the predominant pricing patterns under observed and unobserved demand shocks.⁴⁸ For both $\delta = 0.96$ and 0.76, agents earn higher profits when demand shocks are unobserved, with increases of 2.2% and 8.6%, respectively (p-value = 0 for both). These profit differences suggest that access to demand information increases the incentive to deviate during booms, which may in turn intensify price competition, reduce collusive profits, and enhance consumer welfare.

⁴⁷Even without demand observability, perfect monitoring allows agents to detect deviations and enforce collusive strategies.

⁴⁸Recall that under observed demand shocks, the predominant pricing patterns are Sym-Rigid at $\delta = 0.96$ and Counter-Cycle at $\delta = 0.76$.

	Observed	Unobserved		Observed	Unobserved	
Observed	6.89, 6.89	6.65, 6.65		Observed	3.37, 3.37	1.92, 1.92
Unobserved	6.65, 6.65	7.04, 7.04		Unobserved	1.92, 1.92	3.66, 3.66
	(a) $\delta = 0.96$			(b) $\delta = 0.76$		

Table 7: Payoff Matrices

5.4.2 Asymmetric Information

In reality, firms may adopt different pricing algorithms, raising the question of whether heterogeneous algorithms can still coordinate effectively to sustain supracompetitive profits. Such asymmetry can arise in various forms.⁴⁹ In this paper, I address this question by analyzing a setting in which one agent observes demand shocks while the other does not. This asymmetry may arise when only one firm incorporates demand information into its pricing algorithm.

The simulation results show that at high values of δ , the predominant pricing pattern remains Sym-Rigid for the informed agent (and Sym-1Node for the uninformed agent), with a frequency of 64.3%. This outcome can be attributed to perfect monitoring and the limited incentive for the informed agent to deviate from high prices at H. Moreover, this pricing pattern also passes the deviation tests.

In contrast, at $\delta = 0.76$, the predominant pricing patterns unexpectedly remain Sym-Rigid and Sym-1Node (97.2%), rather than shifting to Counter-Cycle. This finding suggests that a necessary condition for sustaining countercyclical pricing is that both agents observe demand shocks. The mechanism is as follows. When only one agent observes the shocks, the uninformed agent cannot determine whether a price change signals coordination or deviation. To avoid being undercut, the uninformed agent sets low prices. The informed agent follows suit, triggering a price war and resulting in a uniformly low pricing outcome. Thus, countercyclical pricing relies on shared demand observability to ensure mutual interpretability of price movements.

⁴⁹For instance, Brown and MacKay (2023) study a model of price competition in which firms employ different pricing algorithms, with asymmetry stemming from the frequency of price updates.

Table 7 also reports the expected profits under asymmetric information. Compared to the case where both agents observe demand shocks, profits are 3.5% lower when $\delta = 0.96$. The difference is much more pronounced at $\delta = 0.76$, where the average profit drops to 1.92—a substantial decrease of 43.0% (p-value = 0 for both). These results suggest that information symmetry, whether both agents observe or both do not observe demand shocks, is critical for sustaining supracompetitive profits, particularly when agents discount future payoffs more heavily.

6 Conclusion

Motivated by the rise of pricing algorithms and antitrust concerns that the use of nonpublic competitor data may facilitate algorithmic collusion, I study a setting in which firms receive perfect demand forecasts from a common third party that collects and processes their proprietary data, and then embed this demand information into their pricing algorithms. To examine how this information structure influences algorithmic pricing behavior, I build on the framework of Rotemberg and Saloner (1986) and analyze how Q-learning agents interact in a repeated Bertrand competition game with observed demand shocks.

The simulation results demonstrate the robustness of algorithmic collusion under observed demand shocks. In addition, access to such demand information enables Q-learning agents to adapt their pricing strategies to fluctuating market demand, giving rise to distinct pricing patterns. This paper also examines how changes in the information structure—particularly the observability of demand shocks—shape market outcomes. The findings reveal that sharing demand information can reduce profits, suggesting that feeding more information into pricing algorithms may intensify competition and ultimately enhance consumer welfare.

Although this paper advances the understanding of algorithmic collusion in the context of observed demand shocks, much remains to be explored to ensure the robustness of these

findings. In particular, the analysis in this paper assumes that demand shocks are i.i.d., whereas in reality they may be serially correlated, persistent over time, or firm-specific. Moreover, the Bertrand competition framework implicitly assumes instantaneous capacity adjustment and frictionless inventory management. How pricing algorithms perform under more realistic settings warrants further investigation to assess the external validity of the results.⁵⁰

This paper also offers potential policy implications for regulating algorithmic pricing. First, while observing demand shocks may benefit consumers, such results should be interpreted with caution. As Sugaya et al. (2024) show, selective disclosure of demand states can backfire and reduce consumer welfare. These mixed effects underscore the need for a more nuanced understanding of how information sharing should be regulated in the context of algorithmic pricing.

Another potential regulatory direction involves limiting the market power of third-party information intermediaries. This paper finds that symmetric information environments tend to generate higher profits than asymmetric ones. As firms increasingly rely on a common data source, the resulting informational symmetry may facilitate collusive coordination among pricing algorithms. Consistent with this concern, Calder-Wang and Kim (2023) show that markets with greater algorithmic penetration tend to exhibit higher average rents during periods of economic recovery.

Last, as Harrington Jr (2025) emphasizes, the core issue lies not in data sharing *per se*, but in the alignment of objectives. In this paper, each agent is programmed to maximize its long-run expected discounted payoff. In an infinitely repeated environment, such an objective can naturally lead agents—through trial and error—to discover and sustain collusive strategies that yield supracompetitive profits. This concern highlights the need for further examination of the objective functions embedded in pricing algorithms.

⁵⁰For example, Friedrich et al. (2024) study algorithmic collusion in episodic markets with inventory constraints.

Acknowledgement

Computation reported in this work was carried out on the Unity Cluster of the College of Arts and Sciences at the Ohio State University. The computational resources and support provided are gratefully acknowledged.

References

- [1] Abreu, D. (1986). Extremal equilibria of oligopolistic supergames. *Journal of Economic Theory* 39(1), 191–225.
- [2] Assad, S., E. Calvano, G. Calzolari, R. Clark, V. Denicolò, D. Ershov, J. Johnson, S. Pastorello, A. Rhodes, L. Xu, et al. (2021). Autonomous algorithmic collusion: Economic research and policy implications. *Oxford Review of Economic Policy* 37(3), 459–478.
- [3] Assad, S., R. Clark, D. Ershov, and L. Xu (2024). Algorithmic pricing and competition: Empirical evidence from the german retail gasoline market. *Journal of Political Economy* 132(3), 000–000.
- [4] Athey, S., K. Bagwell, and C. Sanchirico (2004). Collusion and price rigidity. *The Review of Economic Studies* 71(2), 317–349.
- [5] Bagwell, K. and R. W. Staiger (1997). Collusion over the business cycle. *The RAND Journal of Economics* 28(1), 82–106.
- [6] Ballesterò, G. (2021). Collusion and artificial intelligence: A computational experiment with sequential pricing algorithms under stochastic costs.
- [7] Barlo, M., G. Carmona, and H. Sabourian (2009). Repeated games with one-memory. *Journal of Economic Theory* 144(1), 312–336.
- [8] Barlo, M., G. Carmona, and H. Sabourian (2016). Bounded memory folk theorem. *Journal of economic theory* 163, 728–774.
- [9] Brown, Z. Y. and A. MacKay (2023). Competition in pricing algorithms. *American Economic Journal: Microeconomics* 15(2), 109–156.
- [10] Calder-Wang, S. and G. H. Kim (2023). Coordinated vs efficient prices: the impact of algorithmic pricing on multifamily rental markets. *Available at SSRN 4403058*.

- [11] Calvano, E., G. Calzolari, V. Denicolò, J. E. Harrington Jr, and S. Pastorello (2020). Protecting consumers from collusive prices due to ai. *Science* 370(6520), 1040–1042.
- [12] Calvano, E., G. Calzolari, V. Denicolo, and S. Pastorello (2020). Artificial intelligence, algorithmic pricing, and collusion. *American Economic Review* 110(10), 3267–3297.
- [13] Calvano, E., G. Calzolari, V. Denicoló, and S. Pastorello (2021). Algorithmic collusion with imperfect monitoring. *International journal of industrial organization* 79, 102712.
- [14] Campbell, J. R. and B. Eden (2014). Rigid prices: Evidence from us scanner data. *International Economic Review* 55(2), 423–442.
- [15] Cho, I. and N. Williams (2024). Collusive outcomes without collusion. *arXiv preprint arXiv:2403.07177*.
- [16] Dolgoplov, A. (2024). Reinforcement learning in a prisoner’s dilemma. *Games and Economic Behavior* 144, 84–103.
- [17] Fish, S., Y. A. Gonczarowski, and R. I. Shorrer (2024). Algorithmic collusion by large language models. *arXiv preprint arXiv:2404.00806*.
- [18] Fonseca, M. A. and H.-T. Normann (2012). Explicit vs. tacit collusion—the impact of communication in oligopoly experiments. *European Economic Review* 56(8), 1759–1772.
- [19] Friedrich, P., B. PÅasztor, and G. Ramponi (2024). Learning collusion in episodic, inventory-constrained markets. *arXiv preprint arXiv:2410.18871*.
- [20] Green, E. J. and R. H. Porter (1984). Noncooperative collusion under imperfect price information. *Econometrica: Journal of the Econometric Society*, 87–100.
- [21] Haltiwanger, J. and J. E. Harrington Jr (1991). The impact of cyclical demand movements on collusive behavior. *The RAND Journal of Economics*, 89–106.

- [22] Hanazono, M. and H. Yang (2007). Collusion, fluctuating demand, and price rigidity. *International Economic Review* 48(2), 483–515.
- [23] Harrington, J. E. (2018). Developing competition law for collusion by autonomous artificial agents. *Journal of Competition Law & Economics* 14(3), 331–363.
- [24] Harrington Jr, J. E. (2025). A critique of recent remedies for third-party pricing algorithms and why the solution is not restrictions on data sharing. *Available at SSRN 5190097*.
- [25] Johnson, J. P., A. Rhodes, and M. Wildenbeest (2023). Platform design when sellers use pricing algorithms. *Econometrica* 91(5), 1841–1879.
- [26] Kandori, M. (1991). Correlated demand shocks and price wars during booms. *The Review of Economic Studies* 58(1), 171–180.
- [27] Klein, T. (2021). Autonomous algorithmic collusion: Q-learning under sequential pricing. *The RAND Journal of Economics* 52(3), 538–558.
- [28] Knittel, C. R. and J. J. Lepore (2010). Tacit collusion in the presence of cyclical demand and endogenous capacity levels. *International Journal of Industrial Organization* 28(2), 131–144.
- [29] Maskin, E. and J. Tirole (1988). A theory of dynamic oligopoly, ii: Price competition, kinked demand curves, and edgeworth cycles. *Econometrica: Journal of the Econometric Society*, 571–599.
- [30] Miklós-Thal, J. and C. Tucker (2019). Collusion by algorithm: Does better demand prediction facilitate coordination between sellers? *Management Science* 65(4), 1552–1561.
- [31] Nuutila, E. and E. Soisalon-Soininen (1994). On finding the strongly connected components in a directed graph. *Information Processing Letters* 49(1), 9–14.

- [32] O'Connor, J. and N. E. Wilson (2021). Reduced demand uncertainty and the sustainability of collusion: How ai could affect competition. *Information Economics and Policy* 54, 100882.
- [33] Rotemberg, J. J. and G. Saloner (1986). A supergame-theoretic model of price wars during booms. *The American Economic Review* 76(3), 390–407.
- [34] Sargent, T. J. and J. Stachurski (2024). *Economic networks: Theory and computation*, Volume 53. Cambridge University Press.
- [35] Sugaya, T., G. Stanford, and A. Wolitzky (2024). Collusion with optimal information disclosure.
- [36] Sugaya, T. and A. Wolitzky (2018). Maintaining privacy in cartels. *Journal of Political Economy* 126(6), 2569–2607.
- [37] Sutton, R. S. (2018). Reinforcement learning: An introduction. *A Bradford Book*.
- [38] Tarjan, R. (1972). Depth-first search and linear graph algorithms. *SIAM Journal on Computing* 1(2), 146–160.
- [39] Watkins, C. J. and P. Dayan (1992). Q-learning. *Machine Learning* 8, 279–292.
- [40] Watkins, C. J. C. H. (1989). Learning from delayed rewards.
- [41] Xu, Z. and W. Zhao (2024). On mechanism underlying algorithmic collusion. *arXiv preprint arXiv:2409.01147*.

Appendix

A Tables

Table A.1: Deviating Agent's Frequencies of Profitable Deviations at $\delta = 0.96$

Stable price	Proportion	Deviation occurring at L									Stable price	Proportion	Deviation occurring at H								
		0.5 ^a	1	1.5	2	2.5	3	3.5	4	4.5			0.5	1	1.5	2	2.5	3	3.5	4	4.5
<i>Panel A: Under Demand Shocks — Sym-Rigid</i>																					
1.5 ^b	0.008	0.13	0.26								1.5	0.008	0.11	0.33							
2	0.272	0.07	0.13	0.20							2	0.272	0.04	0.13	0.36						
2.5	0.346	0.03	0.10	0.12	0.16						2.5	0.346	0.01	0.05	0.15	0.31					
3	0.219	0.03	0.10	0.11	0.12	0.15					3	0.219	0.00	0.04	0.11	0.20	0.29				
3.5	0.095	0.03	0.06	0.09	0.18	0.13	0.17				3.5	0.095	0.00	0.02	0.06	0.22	0.19	0.30			
4	0.043	0.02	0.08	0.08	0.17	0.10	0.16	0.12			4	0.043	0.00	0.05	0.05	0.17	0.16	0.24	0.24		
4.5	0.014	0.02	0.04	0.13	0.11	0.09	0.17	0.06	0.07		4.5	0.014	0.00	0.00	0.07	0.09	0.11	0.25	0.15	0.21	
5	0.002	0.00	0.15	0.33	0.13	0.13	0.12	0.13	0.13	0.00	5	0.002	0.00	0.10	0.00	0.12	0.13	0.14	0.13	0.13	0.10
<i>Panel B: At Single Demand State — Sym-1Node</i>																					
1.5	0.147	0.02	0.13								1.5	0									
2	0.518	0.01	0.06	0.28							2	0.033	0.00	0.06	0.09						
2.5	0.238	0.00	0.05	0.13	0.23						2.5	0.308	0.01	0.01	0.09	0.24					
3	0.077	0.00	0.01	0.13	0.18	0.21					3	0.317	0.01	0.02	0.06	0.09	0.23				
3.5	0.016	0.00	0.07	0.07	0.53	0.33	0.40				3.5	0.202	0.01	0.01	0.04	0.05	0.14	0.17			
4	0.003	0.00	0.00	0.00	0.00	0.00	0.33	0.33			4	0.078	0.00	0.00	0.01	0.01	0.05	0.12	0.17		
4.5	0										4.5	0.042	0.00	0.00	0.05	0.00	0.02	0.17	0.10	0.15	
5	0										5	0.020	0.00	0.00	0.00	0.00	0.05	0.05	0.16	0.11	0.16

Notes: a. The price (row) denotes the undercutting price.

b. The price (column) denotes the stable price before deviation happens.

Table A.2: Deviating Agent's Profit Ratios at $\delta = 0.96$ (Deviation Path Relative to Non-deviation Path)

Stable price	Proportion	Deviation occurring at L									Stable price	Proportion	Deviation occurring at H								
		0.5	1	1.5	2	2.5	3	3.5	4	4.5			0.5	1	1.5	2	2.5	3	3.5	4	4.5
<i>Panel A: Under Demand Shocks — Sym-Rigid</i>																					
1.5	0.008	0.79	0.88								1.5	0.008	0.77	0.94							
2	0.272	0.71	0.78	0.85							2	0.272	0.68	0.81	0.93						
2.5	0.346	0.64	0.71	0.77	0.81						2.5	0.346	0.61	0.72	0.82	0.91					
3	0.219	0.61	0.68	0.73	0.77	0.79					3	0.219	0.57	0.68	0.76	0.84	0.91				
3.5	0.095	0.58	0.65	0.68	0.78	0.74	0.77				3.5	0.095	0.53	0.64	0.70	0.82	0.84	0.91			
4	0.043	0.61	0.67	0.69	0.76	0.73	0.78	0.73			4	0.043	0.54	0.64	0.69	0.79	0.80	0.88	0.89		
4.5	0.014	0.49	0.56	0.65	0.67	0.67	0.78	0.67	0.66		4.5	0.014	0.44	0.52	0.63	0.69	0.73	0.86	0.81	0.85	
5	0.002	0.46	0.61	0.74	0.61	0.64	0.64	0.59	0.52	0.48	5	0.002	0.41	0.57	0.61	0.61	0.68	0.71	0.70	0.72	0.72
<i>Panel B: At Single Demand State — Sym-1Node</i>																					
1.5	0.147	0.69	0.86								1.5	0									
2	0.518	0.66	0.79	0.90							2	0.033	0.61	0.75	0.83						
2.5	0.238	0.61	0.75	0.83	0.90						2.5	0.308	0.60	0.71	0.80	0.89					
3	0.077	0.59	0.73	0.82	0.87	0.91					3	0.317	0.56	0.68	0.76	0.82	0.88				
3.5	0.016	0.68	0.77	0.81	0.96	0.95	0.97				3.5	0.202	0.54	0.63	0.70	0.75	0.82	0.85			
4	0.003	0.56	0.76	0.67	0.72	0.83	0.78	1.08			4	0.078	0.52	0.65	0.66	0.73	0.79	0.85	0.88		
4.5	0										4.5	0.042	0.52	0.61	0.66	0.70	0.75	0.82	0.80	0.85	
5	0										5	0.020	0.52	0.63	0.68	0.74	0.78	0.80	0.88	0.87	0.88

Notes: The settings are identical to those in Table A.1 in Appendix.

B Figures

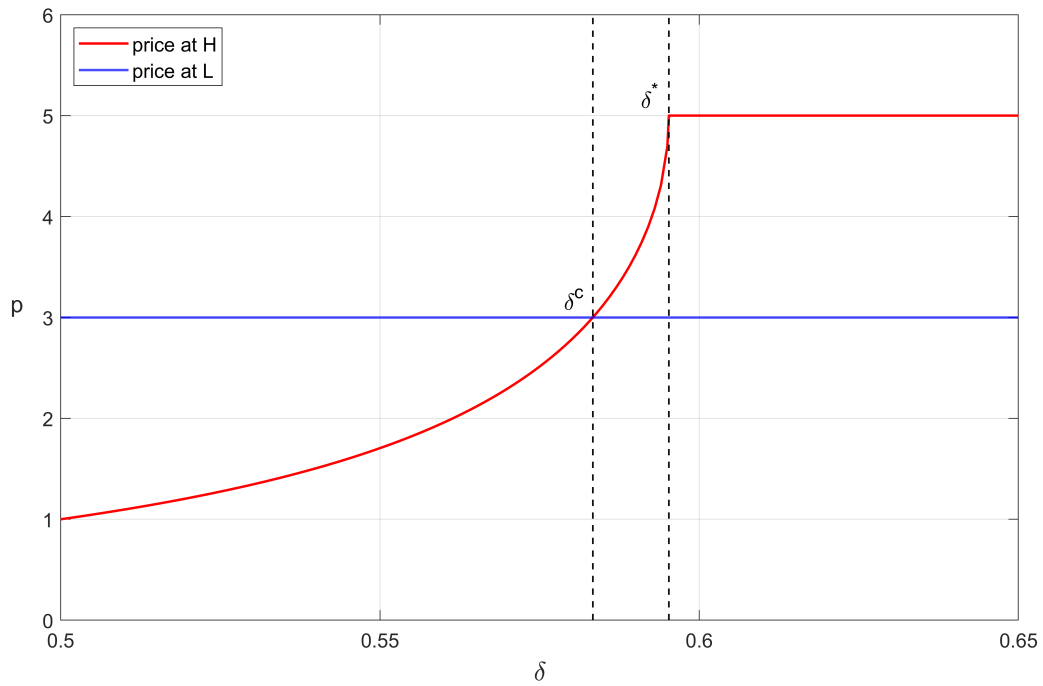


Figure A.1: Predicted Prices for Both Demand States across δ

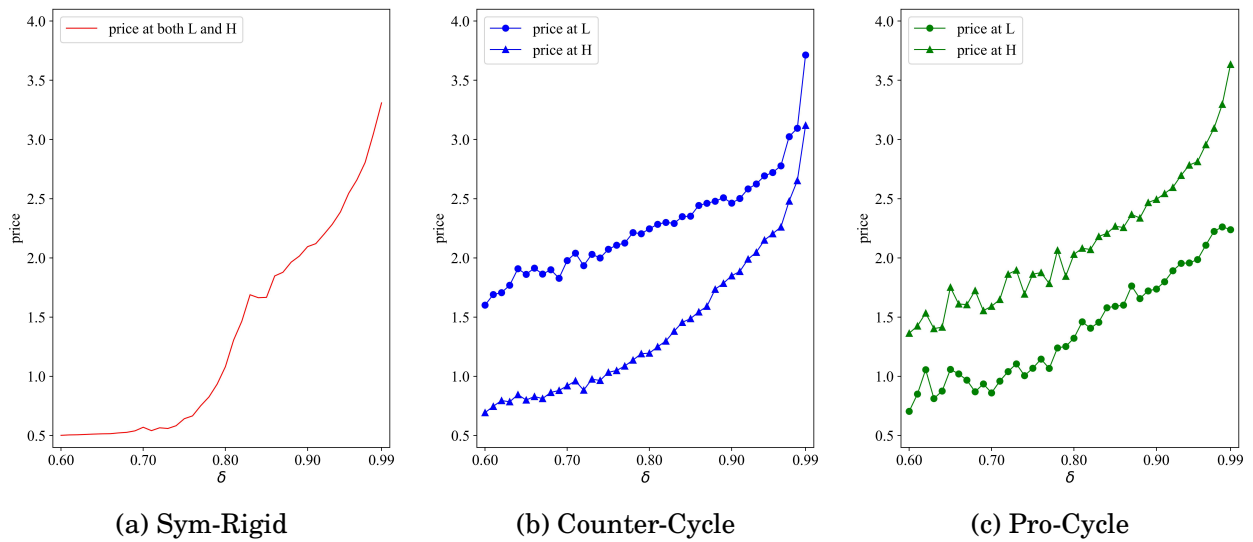


Figure A.2: Price Dynamics of Three Pricing Patterns

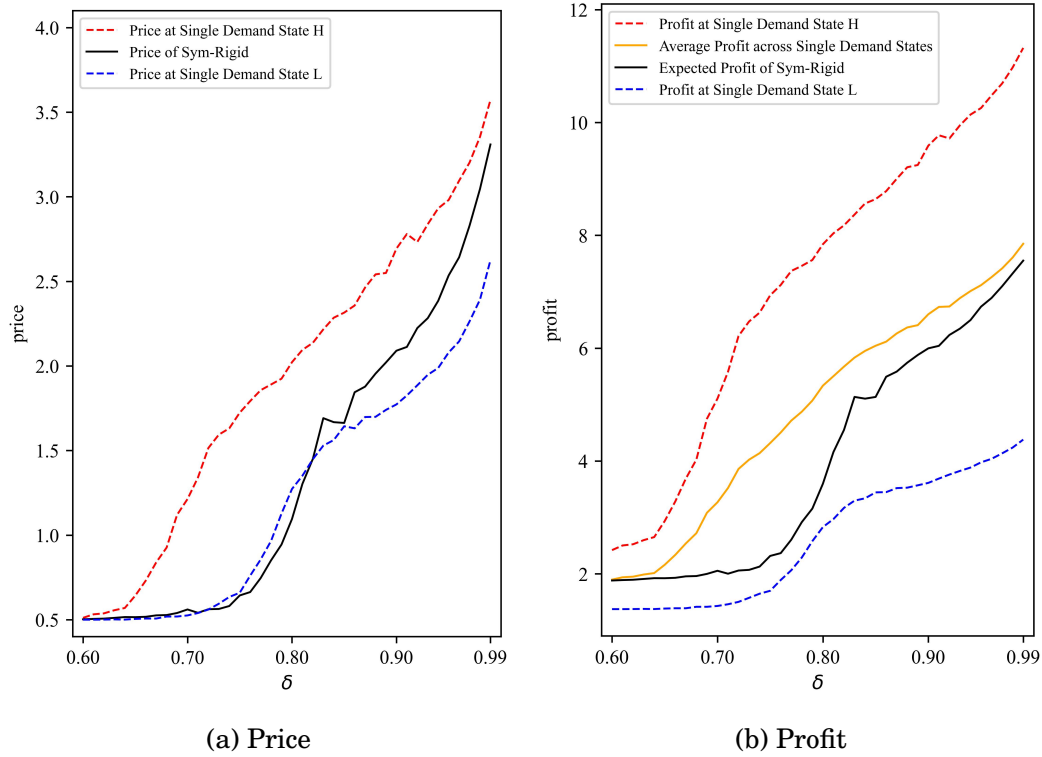


Figure A.3: Price and Profit Dynamics of Sym-Rigid and Sym-1Node

Notes: The black line represents prices and expected profits of Sym-Rigid, while the dashed lines, each in a different color, indicate prices and profits at the single demand states (Sym-1Node). In Panel B, the yellow line represents the average profit across the two single demand states.

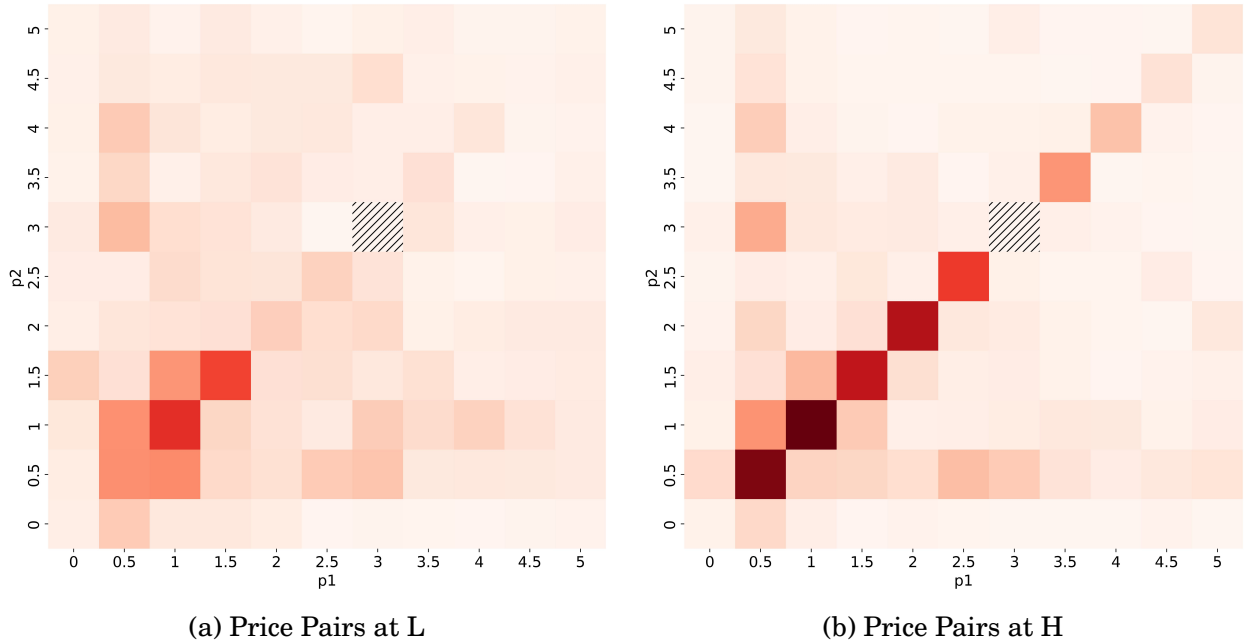


Figure A.4: In-Degree Centrality of Price Pairs on the Deviation Path (Deviation Initiating at L)

Notes: The square depicted in lines marks the pre-deviation price of 3. A deviation initiates when agent 1 undercuts by the minimum price unit after observing a negative demand shock. The color gradient indicates the level of in-degree centrality.

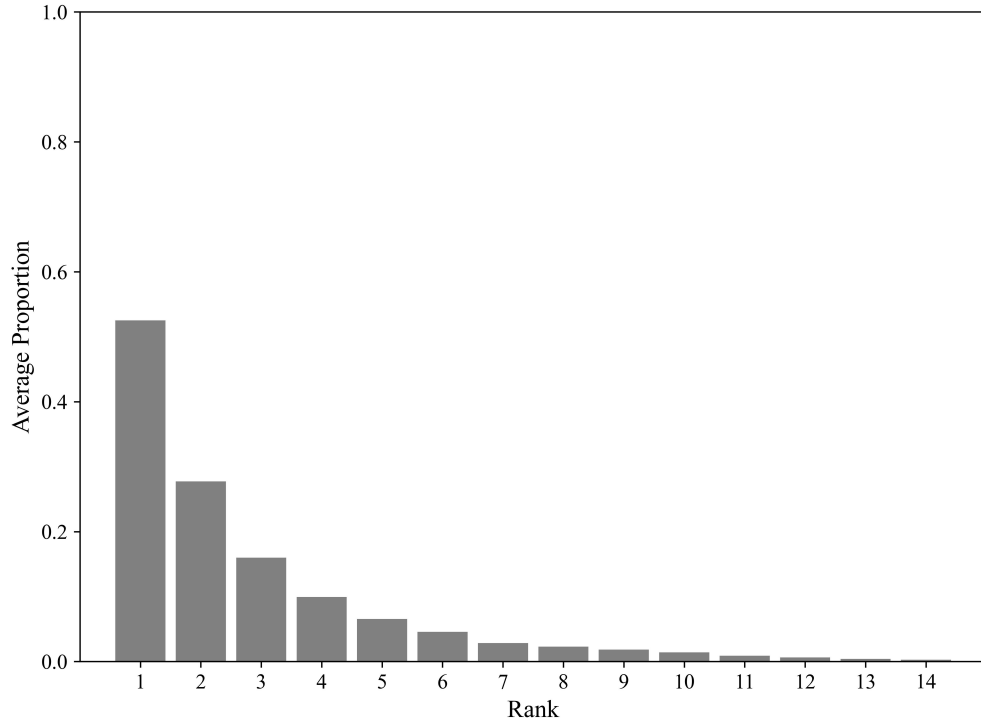


Figure A.5: Average Restart Point Proportions by Rank

Notes: Within each deviation scenario, restart point proportions are ranked in descending order. The average proportion at each rank is then calculated across all deviation scenarios and sessions.

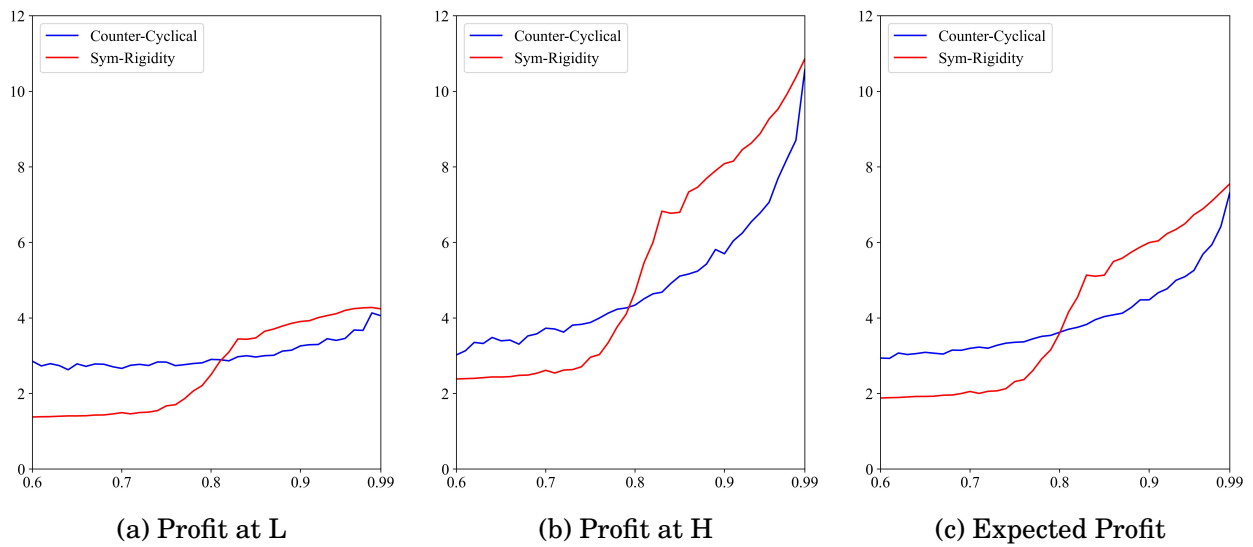


Figure A.6: Profit Comparison: Counter-Cycle vs. Sym-Rigid

C Initial Q-matrix

The initial Q-matrix \mathbf{Q}_{i0} in the baseline setting is calculated as follows. Given that the opponent randomly chooses a price at period $t = 0$, the expected period payoff for agent i who sets price p_i at demand state θ is

$$\bar{\pi}_i(p_i, \theta) = \frac{\sum_{p_{-i} \in A} \pi_i(p_i, p_{-i}, \theta)}{|A|}$$

Correspondingly, the initial Q-value at entry (s_θ, p) , where s_θ denotes any state with demand state being θ , is

$$Q_{i0}(\theta, p_i) = \bar{\pi}_i(p_i, \theta) + \delta \frac{\sum_{\theta_j \in \Theta} Q_{i0}(\theta_j, p_i)}{|\Theta|}$$

where $Q_{i0}(s_\theta, p_i)$ is written as $Q_{i0}(\theta, p_i)$ for simplicity. Thus, the expected continuation value equals the average Q-value of action p_i across all possible demand states.

Then the initial Q-values at p_i for each demand state can be solved through the linear equation system

$$\begin{aligned} Q_{i0}(\theta_1, p_i) &= \bar{\pi}_i(p_i, \theta_1) + \delta \frac{\sum_{\theta_j \in \Theta} Q_{i0}(\theta_j, p_i)}{|\Theta|} \\ Q_{i0}(\theta_2, p_i) &= \bar{\pi}_i(p_i, \theta_2) + \delta \frac{\sum_{\theta_j \in \Theta} Q_{i0}(\theta_j, p_i)}{|\Theta|} \\ &\vdots \qquad \qquad \qquad \vdots \qquad \qquad \qquad \vdots \\ Q_{i0}(\theta_{|\Theta|}, p_i) &= \bar{\pi}_i(p_i, \theta_{|\Theta|}) + \delta \frac{\sum_{\theta_j \in \Theta} Q_{i0}(\theta_j, p_i)}{|\Theta|} \end{aligned}$$

D Theoretical Predictions of Pricing Patterns

Figure A.1 shows the predicted pricing patterns under optimal collusion as δ varies. During negative demand shocks (L), agents charge the monopoly price of 3 as long as $\delta \geq 0.5$. During positive demand shocks (H), there exists two critical values of δ . When $\delta > \delta^* = \frac{25}{42} \approx 0.595$, agents have no incentive to deviate from charging the monopoly price of 5 at H, thus sustaining the fully collusive outcome.⁵¹ When $\delta < \delta^*$, the fully collusive outcome cannot be sustained, leading agents to maintain partial collusion by lowering prices at H.

⁵¹Agents always have a stronger incentive to deviate at H than at L.

When δ lies above the cutoff $\delta^c = \frac{7}{12} \approx 0.583$, procyclical pricing is sustained. In contrast, when δ falls below δ^c , agents further lower prices, resulting in countercyclical pricing. Notably, despite lower prices at H, higher profits are still earned at H when $\delta \in (0.5, \delta^c]$.

E Average Long-run Prices

The transitions on G_c satisfy the Markov property, where each node has exactly two direct successors with equal transition probability of 0.5. Therefore, this defines a finite Markov process. Since G_c is strongly connected, the existence and uniqueness of its stationary distribution are guaranteed. The stationary distribution ψ^* is defined by $\psi^* P = \psi^*$, where P is the stochastic adjacency matrix (Markov matrix).⁵²

Let n denote the number of nodes in G_c . Let $\mathbb{1}_n$ be the $1 \times n$ row vector $(1, \dots, 1)$ and $\mathbb{1}_{n \times n}$ be the $n \times n$ matrix of ones. With I as the identity matrix and P as the stochastic adjacency matrix of G_c , the unique stationary distribution ψ^* can be solved by

$$\mathbb{1}_n = \psi^* (I - P + \mathbb{1}_{n \times n}) \quad (7)$$

Using the stationary distribution ψ^* , the average long-run price for each demand state can be calculated. To illustrate, consider the stochastic adjacency matrix P in Figure 1b:

$$\begin{array}{c} L-(2,2) \quad H-(2,2) \quad H-(4,4) \\ L-(2,2) \left(\begin{array}{ccc} 0.5 & 0 & 0.5 \\ 0.5 & 0 & 0.5 \\ 0.5 & 0.5 & 0 \end{array} \right) \\ H-(2,2) \\ H-(4,4) \end{array}$$

Solving equation (7) yields the stationary distribution $\psi^* = (\frac{1}{2}, \frac{1}{6}, \frac{1}{3})$, where each element represents the steady-state probability of the corresponding node. The average long-run

⁵²The theorem from (34) states that every finite Markov model has at least one stationary distribution ψ^* . If the digraph is strongly connected, then ψ^* is unique and everywhere positive.

price pairs at L and H are (2, 2) and $(\frac{10}{3}, \frac{10}{3})$, respectively.

F Algorithm for Deviation Tests

Algorithm 2 illustrates one simulation in the deviation test. Π_i^* and Π_i^D denote agent i 's accumulated discounted profits on the non-deviation and deviation paths, respectively. The corresponding period profits are denoted by π_{it}^* and π_{it}^D .

Algorithm 2 One Simulation for Deviation Test

First step: Initialization

- 1: θ_0 is realized
- 2: $(\Pi_1^*, \Pi_2^*) \leftarrow (\pi_{11}^*, \pi_{21}^*)$ \triangleright on the non-deviation path
- 3: Let one agent undercut
- 4: $(\Pi_1^D, \Pi_2^D) \leftarrow (\pi_{11}^D, \pi_{21}^D)$ \triangleright on the deviation path

Second step: Loop

- 5: **while** Price dynamics do *not* return to G_c **do**
 - 6: θ_t is realized
 - 7: $(\Pi_1^*, \Pi_2^*) \leftarrow (\Pi_1^* + \delta^t \pi_{1t}^*, \Pi_2^* + \delta^t \pi_{2t}^*)$
 - 8: $(\Pi_1^D, \Pi_2^D) \leftarrow (\Pi_1^D + \delta^t \pi_{1t}^D, \Pi_2^D + \delta^t \pi_{2t}^D)$
 - 9: $t \leftarrow t + 1$
-

G Measuring Commonality in Restart Points

Each deviation scenario is defined by a unique combination of the undercutting price and the demand state at the moment of deviation. Restart points are defined as the combinations of demand state and price pair observed in the final period of the deviation path, immediately before cooperation resumes.

For each deviation scenario, recall that one thousand simulated deviation tests are conducted, thereby allowing all possible restart points to be identified. Let T_i and T_j denote the sets of restart points observed in deviation scenarios i and j within the same session. To measure the degree of commonality in restart points, I use the Jaccard similarity index, defined as

$$J(T_i, T_j) = \frac{|T_i \cap T_j|}{|T_i \cup T_j|}$$

The average pairwise Jaccard similarity within a session is then calculated as

$$\frac{2}{n(n-1)} \sum_{1 \leq i < j \leq n} J(T_i, T_j)$$

where n is the number of deviation scenarios in the session.